ELASTOPLASTIC TOPOLOGY OPTIMIZATION AND CYCLICALLY LOADED STRUCTURES VIA DIRECT METHODS FOR SHAKEDOWN

Mathilde Boissier, Joshua Deaton, Philip Beran, Natasha Vermaak

ELASTOPLASTIC TOPOLOGY OPTIMIZATION AND CYCLICALLY LOADED STRUCTURES VIA DIRECT METHODS FOR SHAKEDOWN

M. BOISSIER[1,2*], J. DEATON[3], P. BERAN[3], N.VERMAAK[4]

[1] *CMAP, École Polytechnique, CNRS UMR7641, Institut Polytechnique de Paris, Palaiseau, France*
[2] *LURPA, ENS Paris-Saclay, Université Paris-Saclay, 94235 Cachan, France*
[3] *U.S. Air Force Research Laboratory, WPAFB, OH, 45433, USA*
[4] *Lehigh University, Mechanical Engineering & Mechanics, 19 Memorial Drive West, Bethlehem, PA 18015-3085 USA*

[*] *mathilde.boissier@cmap.polytechnique.fr*

Abstract: For the first time, the lower bound shakedown theorem is integrated into a level set based topology optimization framework to identify lightweight elastoplastic designs. Shakedown is a cyclic elastoplastic behavior in which, upon cycling beyond the elastic limit, the accumulation of plastic strain arrests and purely elastic behavior is recovered. In contrast to most elastoplastic toplogy optimization, the use of a lower bound shakedown limit allows elastoplastic shakedown limits to be rigorously estimated using only the elastic solution. Under small deformations assumptions, this amounts to solving one simple partial differential equation, avoiding the non-linearity associated with plasticity, and thus simplifying the resolution process. Numerical results are provided for several benchmark examples. The results highlight the design performance enhancements attributed to allowing elastoplastic shakedown to occur instead of designing to first yield. In particular, up to 10% reduction in weight is found for the simple structures considered.

Keywords. Shape optimization, Elastoplastic, Shakedown, Level set method, Direct method

CONTENTS

1 Introduction

Nearly every load-bearing mechanical assembly is loaded more than once in the system lifetime. In many industries, structural materials are designed to withstand repeated variable uni-or-multi-axial proportional or non-proportional loading conditions. The conventional design of these types of structures, that are not limited

by high-cycle fatigue, employs first-yield criteria in order to avoid failure due to cyclic plasticity. Often, these elastic (yield-limited) designs fail to capitalize on the material's load-bearing reserve, leading to inefficiencies related to structural weight and durability. In contrast, designs to shakedown, a safe elastoplastic behavior, may exploit greater component lifetimes enabled by the arrest of plastic accumulation. Within the context of plastic design under variable amplitude loading, shakedown concepts have been utilized in applications as broad as vessels for demilitarization of munitions [92, 91], tribology [85, 63, 106], multilayer systems [9, 109], pavement design [110, 107, 90, 38], shape memory alloy components [77, 108, 93], and nuclear pressure vessels [42, 15, 16, 17, 97, 103, 8, 19, 82]. These and many other applications that are not limited by high cycle fatigue must be designed to avoid cyclic plasticity, i.e. fall in the shakedown regime. Shakedown is a cyclic elastoplastic behavior in which, upon cycling beyond the elastic limit, the accumulation of plastic strain arrests (due to the formation of residual stresses) and purely elastic behavior is recovered (Fig. 1). In this way, shakedown designs can replace traditional yield-limited assessments of structural integrity and shakedown analyses can be used to evaluate structural response to unanticipated loads. While shakedown concepts, powerful limit theorems, and numerical methods have been developed since the 1920s and 1930s [37, 12, 64, 65, 103], they are severely underutilized, especially in modern structural optimization.

This article presents, for the first time, the integration of the lower bound shakedown theorem into a level set based topology optimization framework to identify lightweight elastoplastic designs. In contrast to most elastoplastic topology optimization, the use of constraints based on a lower bound shakedown theorem in the present work allows elastoplastic shakedown limits to be rigorously estimated *using only the elastic solution*. The framework is applied to metallic structures subject to repeated loads and elastoplastic shakedown designs are compared against designs to first-yield. Under conditions in which loading levels are known, designing to shakedown should provide greater lightweighting benefits than designing to first-yield. Under conditions in which loading levels are uncertain (within a prescribed envelope), designing to shakedown should provide greater durability at more extreme loading levels than designs to first yield. The term *shakedown* was first used by W. Prager [87, 95], referring to the established shakedown limit theorems from Bleich and Melan [12, 64, 65] that determines whether a structure can safely carry a set of external loads whose maximum and minimum values only are known. One of the major advantages of these bounding shakedown theorems as "Direct Methods" is that information about the loading path in an arbitrarily complex loading space is not needed [103, 98]. In contrast, the "classical load history approach" follows the incremental or step-by-step evolution of a system and finds the actual state variable fields that would result from the actual loading history that is deterministically known. "Classical incremental or load history approaches" and "Direct Methods" are complementary methods – each providing different information for often separate domains of applicability.

Many authors have considered elastoplastic stress-based shape or topology optimization in the past, but a vast majority of these have tackled the more computationally demanding classical incremental load-history based approaches. Some notable examples of including material non-linearity effects through plasticity in shape and topology optimization include [62, 40, 31, 44, 89, 88, 75, 67, 57, 7, 49, 61]. To the best of the authors' knowledge, only [104, 105, 48, 47, 96, 35, 34, 11, 72] have specifically addressed the shape and topology optimization of structures under shakedown behavior. None of these have leveraged the level set method for topology optimization as will be shown here. Moreover, one of the main contributions of the present work is in reimagining the way in which Melan's theorem can be adapted to modern topology optimization formulations. The only other studies in which elastoplastic shakedown constraints have been imposed have pursued more literal adaptations that fail to capitalize on the mathematical freedom granted by Melan's powerful theorem.

Considering shakedown constraints in shape optimization is of high interest. Indeed, optimizations that seek to avoid plastic response can be considered special cases of optimization for shakedown behavior. Optimizing under shakedown constraints thus gives more freedom in the design process. Besides proposing a level set formulation including shakedown in shape optimization problems, this work is mainly aimed at illustrating the benefits of shakedown and motivating its application with numerical examples and comparison of shape optimization under shakedown, first-yield and other related constraints. There are many challenges that have been documented as associated with stress-based (the "singularity phenomena" for SIMP-based stress-constrained problems [25, 28, 29, 79, 18, 74, 53], the local nature of stress constraints [4, 30, 53, 27, 73, 45], highly non-linear dependencies of stress constraints on the design [100, 39, 99, 10, 53], etc.). However, the focus here is not to optimize algorithm performance with respect to these challenges. Instead, the numerical choices, detailed below, are kept simple to clearly present the influence of shakedown constraints through algorithm adaptations and the corresponding results.

The article is organized in the following way. First, in Section 2, the background and use of shakedown theorems is developed. These theorems and especially Melan's lower bound theorem, allows one to identify asymptotic structural behavior without following the entire loading history [64, 50]. This simpler formulation involves only one linear elastic partial differential equation instead of a full elastoplastic history resolution, facilitating the theorem's incorporation into the optimization protocol. Section 3 gives a first straightforward formulation of the optimization problem and highlights two difficulties associated with this initial formulation.

First, the Von Mises constraints are pointwise, creating large computational demand, depending on the mesh definition. This pointwise issue, which is well-known in shape optimization under elastoplastic constraints, has been faced by many authors [7, 53, 55, 79, 81]. We have chosen here to follow mitigation suggestions made by Amstutz and Novotny [7] – detailed in Section 3.1. Secondly, the shakedown theorem requires the existence of a self-equilibrated stress. To deal with the existence issue for this self-equilibrated stress, the stress is considered as an optimization variable. To deal with the necessity of satisfying the self-equilibrating constraint, the orthogonal projection from the stress space to self-equilibrated stress spaces will be introduced. These modifications lead to a final optimization problem, the solution algorithm, and numerical applications. Section 4 introduces the shape optimization theory required for the numerical applications [6, 43] and provides an overview of the level set method [5]. Section 5 compares three potential test-cases applied to two benchmark problems (the classic cantilever and L-bracket) in 2D under plane stress conditions. These test-cases are used to highlight the influence of the shakedown constraint. Some assume a perfectly elastic material, and in others a constraint on designing to first-yield for an elastic-perfectly plastic material is assumed. Finally, an elastic-perfectly plastic material is used while including a shakedown constraint. In comparing the results, the impact of the different constraints is elucidated. It should be noted that the restriction to 2D is without loss of generality and the methods developed herein could easily be extended to 3D.

2 Elastoplastic Shakedown Theorems

We will focus on materials and conditions that admit time-independent classical plasticity formulations and an elastic-perfectly plastic material model. There are numerous plasticity textbooks and monographs that outline shakedown behavior and the bounding shakedown theorems (lower and upper bound theorems) and their proofs formalized by W.T. Koiter [50] and others [56, 23, 60, 51]. In the present work, focus will be on one of the most common "Direct Methods" for shakedown determination – Melan's Lower Bound Theorem.

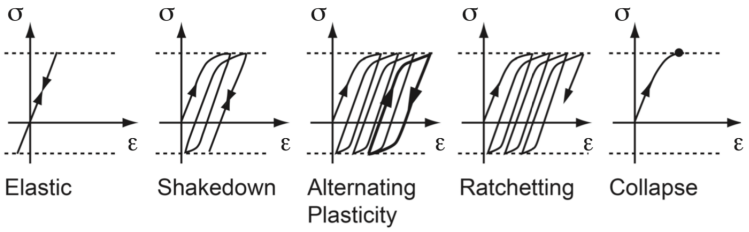

Figure 1: Schematic representation of cyclic elastoplastic behaviors.

2.1 Melan's Quasi-Static Lower Bound Theorem for Shakedown Limit Loads

In its original form, Melan's assumptions include small deformation theory, elastic perfectly plastic constitutive laws for associated plastic flow and convex yield surfaces, quasi-static structural response, body forces and surface tractions that can vary arbitrarily and independently, material properties that are temperature-independent, and negligible time-dependent effects such as creep and rate-sensitivity [50, 52, 64, 65]. It should be noted that this theorem has since been extended to relax and address all of these initial restrictions — i.e. to analyze temperature-dependent properties, hardening, creep, damage, nonlinear geometry effects, and others [78, 76, 24, 13, 1, 54, 102, 101, 80, 103]. The original theorem [50, 14] states that:

> *If any time-independent distribution of residual stresses, $\bar{\rho}_{ij}$, can be found such that the sum of these residual stresses and the "elastic" stresses, σ^e_{ij}, is a safe state of stress $\sigma^e_{ij} + \bar{\rho}_{ij} = \sigma^s_{ij}$, i.e. a state of stress inside the yield limit, at every point of the body and for all possible load combinations within the prescribed bounds, then the structure will shake down to some time-independent distribution of residual stresses (usually depending on the actual loading program), and the response to subsequent load variations within the prescribed limits will be elastic. On the other hand, shakedown is impossible if no time-independent distribution of residual stresses can be found with the property that the sum of the residual stresses and "elastic" stresses is an allowable state of stress at every point of the body and for all possible load combinations.*

Thus, to ensure that a structure will shakedown, a residual stress field, ρ, must be found that satisfies the following three conditions: (i) it has to be self-equilibrating, (ii) it has to be time-independent, and (iii) it has to remain within the yield stress limit when combined with any fictitious "elastic" stress caused by a load combination from the loading domain. This powerful theorem gives a necessary and sufficient condition

to determine if a structure will shakedown or not. The proof for Melan's lower bound theorem relies on consideration of strain energies, the principle of virtual work, and the postulate of maximum plastic dissipation [14, 94, 50, 51].

The use of constraints based on the lower bound shakedown theorem in the present work allows elastoplastic shakedown limits to be rigorously estimated *using only the elastic solution*. As a result, the computational complexity is significantly reduced compared to classical elastoplastic topology optimization approaches. For typical elastoplastic topology optimization, the actual stresses corresponding to the choice of loading, boundary conditions and material model must be found. In the case of cyclic loading, in addition, the actual residual stress field must also be determined. Even if this residual stress field can be found from the solution of a partial differential equation [78], the associated computational costs are high, let alone incorporating this calculation within an optimization process. Moreover, changing the loading history (even staying within the same prescribed loading domain) would completely change the actual residual stress field and the optimization process would have to start all over again. While the use of the lower-bound theorem in the present work avoids these issues, the drawback is that we don't have any information about the actual residual stress field developing in the solid. Indeed, this theorem only requires the existence of a residual stress field and doesn't state anything about its uniqueness. Nevertheless, topology optimization can be performed with constraints on the cyclic elastoplastic behavior (ensuring shakedown) based on much simpler computations for elastic solutions.

In the following, all of the assumptions for Melan's Lower bound theorem outlined above are applied. Most importantly, an isotropic linearly elastic perfectly plastic material model that is relevant for many structural steels is assumed and the von Mises equivalent stress is used to define the yield function. For convenience, only surface loadings and no volumetric or thermal loads are considered.

2.2 Problem Description

Consider a design domain $D \subset \mathbb{R}^2$ and a space of admissible shapes $\mathscr{U}_\Omega$. Let the shape, which is an element of the admissible shapes $\Omega \in \mathscr{U}_\Omega$, be an open bounded set such that $\Omega \subset D$. Its boundary, $\partial\Omega$, characterized by its normal, n, is composed of three disjoints parts (Fig. 2): Γ_D on which displacement is imposed (Dirichlet boundary condition), Γ_N on which any load could be applied, and Γ which is traction-free. Only the boundary Γ is optimizable and the boundary Γ_D is assumed not to be reduced to the empty set ($\Gamma_D \neq \emptyset$).

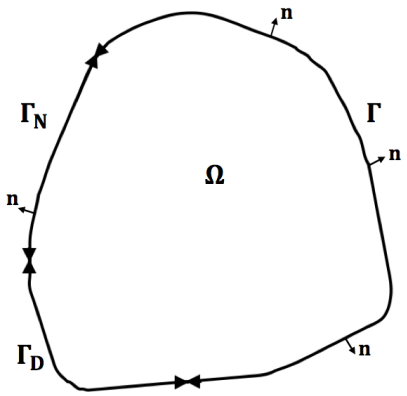

Figure 2: Open set Ω

The solid (and corresponding shape Ω) is comprised of an isotropic linear elastic and perfectly plastic material with a generalized Hooke's tensor A relating the elastic stress and strain. Recall that for any symmetric matrix ξ, A is defined by:

$$A\xi = \frac{E}{1-\nu^2}\left((1-\nu)\xi + \nu \mathrm{Tr}(\xi)\right) I_2, \tag{1}$$

where E is the Young's modulus, ν is Poisson's ratio and I_2 is the identity tensor in two dimensions. In particular, with linearized elasticity, the elastic stress σ^e, elastic strain e, and the elastic displacement u are defined such that:

$$e(u) = \frac{1}{2}\left(\nabla u + {}^t\nabla u\right), \qquad \sigma^e = Ae(u). \tag{2}$$

where ^{t} denotes the transpose operation.

A von Mises yield criterion is chosen to represent the onset of plastic yielding and is characterized by a function σ_{VM}, given by eq. (3) [7, 61]:

$$\sigma_{VM}(\sigma) = \sigma_D : \sigma_D, \qquad \sigma_D = \sigma - \frac{\mathrm{Tr}(\sigma)}{2} I_2. \tag{3}$$

The domain of elasticity is given by eq. (4), where $\mathscr{S}_{2\times 2}\left(L^2(D)\right)$ represents the space of symmetric two-dimensional tensors whose components are in $L^2(D)$:

$$\mathscr{E}(\Omega) = \{\sigma \in \mathscr{S}_{2\times 2}\left(L^2(D)\right), \quad \text{such that} \quad \forall x \in \Omega,\ \sqrt{\sigma_{VM}(\sigma)} - \sigma_Y \leq 0\}. \tag{4}$$

where σ_Y is the yield stress. The surface loading applied to the Neumann boundary, Γ_N, is denoted g and belongs to the loading domain $\mathscr{G}$, defined by eq. (5):

$$\mathscr{G} = \{\tau G_{min} + (1-\tau)G_{max},\ \tau \in [0,1]\}, \tag{5}$$

where $G_{min}, G_{max} \in \mathbb{R}$ are extremal loadings ($G_{min} \leq G_{max}$).

Two different stresses are to be distinguished: (i) the "actual" stress σ^a resulting from the elastoplastic behavior of the solid Ω under the prescribed loads and (ii) the "fictitious" elastic stress σ^e which would result in Ω under the same loading conditions if the solid was comprised of a purely elastic material. The elastic displacement $u \in H^1(\Omega)$ corresponding to this fictitious elastic stress σ^e (see (2)) is the solution of the partial differential equation given by eq. (6):

$$\begin{cases} -\text{div}\left(Ae(u)\right) = 0 & \text{in}\,\Omega \\ Ae(u).n = g & \text{on}\,\Gamma_N \\ Ae(u).n = 0 & \text{on}\,\Gamma \\ u = 0 & \text{on}\,\Gamma_D. \end{cases} \tag{6}$$

Setting $H^1_D(\Omega) = \{v \in H^1(\Omega),\ \text{such that}\ v = 0\ \text{on}\ \Gamma_D\}$ the space of the function in $H^1(\Omega)$ cancelling on Γ_D, the elastic variational problem states that, $\forall \varphi \in H^1_D(\Omega)$,

$$\int_\Omega Ae(u) : e(\varphi)dx - \int_{\Gamma_N} g\varphi ds = 0. \tag{7}$$

It is well known that the elastic problem, eq. (6), is well-posed if $\Gamma_D \neq \emptyset$, and that the equation will admit a unique weak solution $u \in H_1(\Omega)$ [32].

2.3 Adaptation of Melan's Lower Bound Shakedown Theorem

In this context, the von Mises yield function $\sigma \mapsto \sqrt{\sigma_{VM}(\sigma)}$ is convex and the loading domain $\mathscr{G}$ is also a convex hull with two corners, G_{min} and G_{max}. Following [98], Melan's theorem can be restated for adaptation in a topology optimization framework:

A structure, Ω, (see Fig.2) subjected to any cyclic traction g in the loading domain $\mathscr{G}$ applied on the Neumann boundary, Γ_N, will shakedown under this loading domain if one can find a stress field ρ, satisfying :

- *a **self-equilibrating condition**: the divergence of this stress field ρ over the solid, Ω is zero and no traction is applied on the solid's boundary $\Gamma \cup \Gamma_N$ ([14]):*

$$\begin{cases} div(\rho) = 0 & in\,\Omega \\ \rho \cdot n = 0 & on\,\Gamma \cup \Gamma_N \end{cases} \tag{8}$$

- *a **pointwise safe-state condition**: at each point x in the solid, the superposition of the stress $\rho(x)$ with the fictitious elastic stress, $\sigma^e(x)$, corresponding to any loading corner (G_{min} or G_{max}) in the loading domain, $\mathscr{G}$, is a safe state of stress. Relating these fictitious stresses to the elastic displacements, u_{min} and u_{max}, these pointwise conditions are given by eq.* (9)*:*

$$\forall x \in \Omega, \begin{cases} \sigma_{VM}\left(\rho(x) + Ae(u_{min})(x)\right) \leq \sigma_Y^2, \\ \sigma_{VM}\left(\rho(x) + Ae(u_{max})(x)\right) \leq \sigma_Y^2. \end{cases} \tag{9}$$

where u_{min} and u_{max} are the solution of eq. (6)*, with a traction loading of G_{min} and G_{max}, respectively.*

For convenience and to simplify notation, we consider in the following that $G_{min} = 0$ and $G_{max} = g$. Thus, $u_{min} = 0$ and we will write $u_{max} = u$.

3 Optimization Problem

Based on Section 2.3, a first straightforward formulation of the optimization problem is given by eq. (10):

$$\min_{\Omega\in\mathscr{U}_\Omega} J(\Omega)$$
$$\text{such that } \left\{ \begin{array}{l} \exists \rho \in K = \left\{ \mathscr{S}_{2\times 2}\left(L^2(D)\right) \text{ such that } \left\{ \begin{array}{ll} \text{div}\rho = 0 & \text{in}\,\Omega \\ \rho\cdot n = 0 & \text{on}\,\Gamma\cup\Gamma_N \end{array} \right. \right\} \\ \forall x\in\Omega, \left\{ \begin{array}{l} \sigma_{VM}\left(\rho(x)\right) \leq \sigma_Y^2, \\ \sigma_{VM}\left(\rho(x) + A\left(e\left(u(x)\right)\right)\right) \leq \sigma_Y^2, \end{array} \right. \end{array} \right. \tag{10}$$

with $J\in\mathscr{C}^1(\mathscr{U}_\Omega,\mathbb{R})$ representing the objective function. Note that considering $\mathscr{S}_{2\times2}(L^2(D))$ or $\mathscr{S}_{2\times2}(L^2(\Omega))$ amounts to the same: we are only interested in the residual stress within the domain Ω and this stress can easily be extended by 0 in $D\setminus\bar{\Omega}$. In the following, we consider $\mathscr{U}_{\tilde{\rho}}$ the space of admissible stresses defined on Ω (or equivalently defined on D extending the stress by 0 on $D\setminus\Omega$),

$$\mathscr{U}_{\tilde{\rho}} = \mathscr{S}_{2\times2}(L^2(\Omega)) = \{\tilde{\rho}\in\mathscr{S}_{2\times2}(L^2(D)) \text{ such that } \tilde{\rho}=0 \text{ in } D\setminus\bar{\Omega}\}. \tag{11}$$

It would be possible to add other equality and inequality constraints but, for the sake of simplicity, none are added at this time.

Two difficulties arise from this formulation (eq. (10)). First, the safe-state constraints are pointwise (eq. (9)) and their number is related to the mesh definition. This creates a large computational demand and a strategy for mitigating computation costs related to the pointwise constraints is needed to maintain a tractable optimization formulation. Second, and perhaps more troublesome, the shakedown constraint is based on the existence of a stress satisfying both self-equilibrating (eq. (8)) and safe-state properties (eq. (9)). This "existence problem" must be transformed to be included in the optimization process. Both of these issues are addressed below.

3.1 Dealing with pointwise constraints

The pointwise issue is quite common in shape optimization under von Mises constraints [7, 53, 55, 79, 81]. In this work, we follow the strategy of Amstutz and Novotny [7] and a functional Φ_p is introduced ($p\in\mathbb{N}$):

$$\Phi_p : \left\{ \begin{array}{l} \mathbb{R}_+ \to \mathbb{R}_+ \\ t \mapsto \left(1+t^p\right)^{1/p} - 1. \end{array} \right. \tag{12}$$

This functional is non-negative, non-decreasing and $\mathscr{C}^2(\mathbb{R})$. Moreover, it admits sharp variations around 1. The pointwise constraints are thus reduced to:

$$\begin{array}{l} C_0(\Omega,\rho) = \int_\Omega \Phi_p\left(\frac{\sigma_{VM}(\rho(x))}{\sigma_Y^2}\right) dx = 0, \\ C_M(\Omega,\rho) = \int_\Omega \Phi_p\left(\frac{\sigma_{VM}(\rho(x)+Ae(u(x)))}{\sigma_Y^2}\right) dx = 0. \end{array} \tag{13}$$

Figure 3 presents the graph of Φ_p for different values of p, reproduced from Amstutz and Novotny [7]. We notice that small von Mises stress variations result in huge variations in the function Φ_p where the von Mises stresses are greater than the yield stress. As long as the von Mises stresses are less than the yield stress, the function Φ_p remains close to 0; the accuracy depends on the power p ($p=8$ or $p=16$ is used in the numerical examples below). For further detail, the reader is referred to Amstutz and Novotny [7]. Finally, to simplify the notation, the dependence of the stresses on x within the safe-state constraint integrals are, from now on, omitted.

3.2 Dealing with the self-equilibrating constraints

To address the "existence problem" outlined above, the residual stress ρ is added to the optimization variables. The resulting problem is to find the couple $(\Omega,\rho)\in\mathscr{U}_\Omega\times K$ that minimizes the objective function J while satisfying the constraint $C_0(\Omega,\rho)=0$, $C_M(\Omega,0)=0$, with K the space of self-equilibrated stresses:

$$K = \left\{\rho\in\mathscr{U}_{\tilde{\rho}}, \text{such that } \text{div}(\rho)=0 \text{ in } \Omega, \text{ and } \rho\cdot n = 0 \text{ on } \Gamma\cup\Gamma_N\right\}. \tag{14}$$

This is one of the main contributions of the present work: in reimagining the way in which Melan's theorem can be adapted to modern topology optimization formulations. The only other studies in which elastoplastic shakedown constraints have been imposed have pursued more literal adaptations that fail to capitalize on the mathematical freedom granted by Melan's powerful theorem.

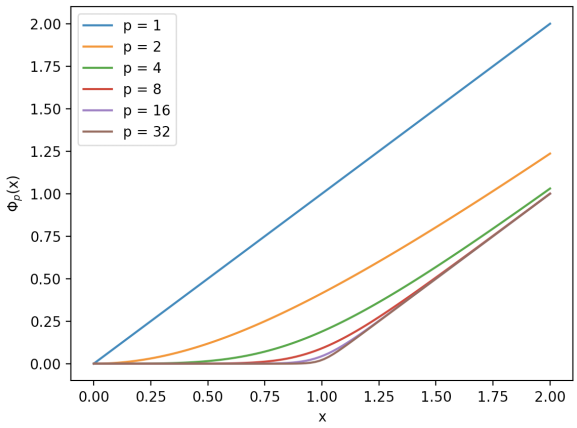

Figure 3: Function Φ_p for $p = 1, 2, 4, 8, 16, 32$, from [7].

To deal with the constraint $\rho \in K$, we consider the Hilbert space $\mathscr{U}_{\tilde{\rho}}$ to which we assign the scalar product a_ρ such that:

$$\forall \tilde{\rho}, \tilde{\rho}' \in \mathscr{U}_{\tilde{\rho}}, \qquad a_{\tilde{\rho}}(\tilde{\rho}, \tilde{\rho}') = \int_D \tilde{\rho} : \tilde{\rho}' dx. \tag{15}$$

Then, we define $\tilde{K} \subset \mathscr{U}_{\tilde{\rho}}$ as a space of strains such that:

$$\tilde{K} = \{e(\eta), \eta_{|\Omega} \in H^1(\Omega), \eta = 0 \text{ on } \partial\Omega, \text{ such that } \eta = 0 \text{ in } D \setminus \bar{\Omega}\}. \tag{16}$$

Lemma 3.1. *Let Ω be a bounded and Lipschitz open set. Then*

$$\mathscr{U}_{\tilde{\rho}} = K \oplus \tilde{K}. \tag{17}$$

Proof. Set $\rho \in K \subset \mathscr{U}_{\tilde{\rho}}$ and $\varepsilon \in \tilde{K} \subset \mathscr{U}_{\tilde{\rho}}$. Then, there exists $\eta \in H^1_D(\Omega)$ such that $\varepsilon = e(\eta)$. Then,

$$\begin{array}{ll} a_{\tilde{\rho}}(\rho, \varepsilon) & = \int_D \rho : e(\eta) dx \\ & = -\int_\Omega \mathrm{div}\rho \cdot \eta dx - \int_{\Gamma \cup \Gamma_N} \rho \cdot n \eta ds - \int_{\Gamma_D} \rho \cdot n \eta ds \\ & = 0. \end{array}$$

Thus, these two spaces are orthogonal with respect to the scalar product $a_{\tilde{\rho}}$.

Set $\tilde{\rho} \in \mathscr{U}_{\tilde{\rho}}$ and $\eta \in H^1(\Omega)$ solution of:

$$\left\{ \begin{array}{ll} \mathrm{div}(e(\eta)) = \mathrm{div}(\tilde{\rho}) & \text{in } \Omega \\ e(\eta) \cdot n = \tilde{\rho} \cdot n & \text{on } \Gamma \cup \Gamma_N \\ \eta = 0 & \text{on } \Gamma_D \end{array} \right. \tag{18}$$

The strain η can be extended by 0 to $H^1(D)$. Then, $\rho = \tilde{\rho} - e(\eta) \in K$ and $e(\eta) \in \tilde{K}$ and thus, $\tilde{\rho} = \rho + e(\eta)$, which concludes the proof. □

□

This lemma leads to the definition of the unique orthogonal projection P_K on the vector space K:

$$P_K : \left\{ \begin{array}{ccc} \mathscr{U}_{\tilde{\rho}} & \to & K \\ \tilde{\rho} & \mapsto & \rho = \tilde{\rho} - e(\eta_{\tilde{\rho}}) \end{array} \right. \tag{19}$$

with $\eta_\rho \in H^1(\Omega)$ as the solution of:

$$\left\{ \begin{array}{ll} \mathrm{div}\,(e(\eta_{\tilde{\rho}})) = \mathrm{div}\tilde{\rho} & \text{in } \Omega \\ e(\eta_{\tilde{\rho}}) \cdot n = \tilde{\rho} \cdot n & \text{on } \Gamma \cup \Gamma_N \\ \eta_{\tilde{\rho}} = 0 & \text{on } \Gamma_D, \end{array} \right. \tag{20}$$

extended to 0 in $D \setminus \bar{\Omega}$. Optimizing the shape under the existence of a self-equilibrated constraint has thus been *transformed into optimizing both the shape and the stress $\tilde{\rho}$, by projecting it on the self-equilibrated stress space* (see Figure 4).

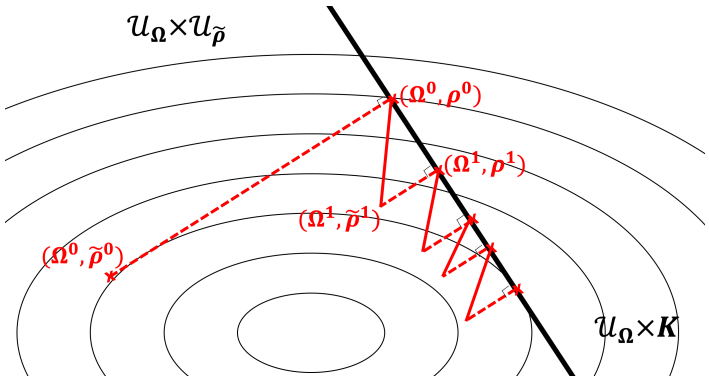

Figure 4: Schematic of projected gradient process: the optimization variables are first modified with respect to the gradient (orthogonal to its level sets) and then projected onto the set K.

3.3 Final optimization problem formulation

From the simplifications above in Sections 3.2 and 3.1, a final formulation of the optimization problem is:

$$\begin{aligned} &\min_{\Omega \in \mathscr{U}_\Omega \tilde{\rho} \in \mathscr{U}_{\tilde{\rho}}} J(\Omega) \\ &\text{such that} \\ &\begin{cases} \rho = \tilde{\rho} - e(\eta) \\ C_0(\Omega, \rho) = \int_\Omega \Phi_p \left(\frac{\sigma_{VM}(\rho)}{\sigma_Y^2} \right) dx = 0, \\ C_M(\Omega, \rho) = \int_\Omega \Phi_p \left(\frac{\sigma_{VM}(\rho + Ae(u))}{\sigma_Y^2} \right) dx = 0. \end{cases} \end{aligned} \tag{21}$$

or equivalently:

$$\begin{aligned} &\min_{\Omega \in \mathscr{U}_\Omega \tilde{\rho} \in \mathscr{U}_{\tilde{\rho}}} J(\Omega) \\ &\text{such that} \\ &\begin{cases} C_0(\Omega, \tilde{\rho}) = \int_\Omega \Phi_p \left(\frac{\sigma_{VM}(\tilde{\rho} - e(\eta))}{\sigma_Y^2} \right) dx = 0, \\ C_M(\Omega, \tilde{\rho}) = \int_\Omega \Phi_p \left(\frac{\sigma_{VM}(\tilde{\rho} - e(\eta) + Ae(u))}{\sigma_Y^2} \right) dx = 0. \end{cases} \end{aligned} \tag{22}$$

with $u \in H^1(\Omega)$ the solution of:

$$\begin{cases} -\text{div}\,(Ae(u)) = 0 & \text{in}\,\Omega \\ Ae(u) \cdot n = g & \text{on}\,\Gamma_N \\ Ae(u) \cdot n = 0 & \text{on}\,\Gamma \\ u = 0 & \text{on}\,\Gamma_D. \end{cases} \tag{23}$$

and $\eta \in H^1(\Omega)$ the solution of:

$$\begin{cases} \text{div}\,(e(\eta)) = \text{div}\tilde{\rho} & \text{in}\,\Omega \\ e(\eta) \cdot n = \tilde{\rho} \cdot n & \text{on}\,\Gamma \cup \Gamma_N \\ \eta = 0 & \text{on}\,\Gamma_D. \end{cases} \tag{24}$$

In the following, the objective function is to minimize mass (here the volume) penalized by the compliance (chosen to avoid $\Omega = \emptyset$):

$$J(\Omega) = \int_\Omega dx + l_C \int_\Omega Ae(u) : e(u) dx. \tag{25}$$

In the numerical applications, this l_C will be arbitrarily chosen depending on the test case and kept fixed during the optimization.

Remark 3.1. *Note that, to avoid the empty set, it would also have been possible to replace the volume minimization function by a function penalizing volumes different from a target value. With the goal of emphasizing the role of shakedown constraints in light-weighting, the compliance approach is preferred.*

4 Shape Optimization

To solve the optimization problem (eq. (22)), a gradient-based algorithm is adopted. Consequently, the above functions must be differentiated with respect to the shape Ω and to the stress $\tilde{\rho}$. While performing the derivatives involving $\mathscr{U}_{\tilde{\rho}}$ are quite intuitive, shape optimization theory must be introduced to compute the shape derivatives with respect to Ω. This is done in the following Section 4.1. In addition, a representation of the shape must be chosen for numerical purposes. The level-set method, adopted in this work, is detailed in the subsequent Section 4.2.

4.1 Shape differentiation

First introduced by Hadamard, shape differentiation theory has been widely developed. We shall use the analysis of Murat and Simon [3, 43, 68]. Consider a smooth reference set Ω_0. Any admissible shape Ω is assumed to be related to the reference shape through a perturbation θ such that:

$$\Omega = \{x + \theta(x) \text{ such that } x \in \Omega_0\}. \tag{26}$$

To limit the shape's deformation, the vector field must be taken in $W^{k,\infty}\left(\mathbb{R}^d, \mathbb{R}^d\right)$, with k being fixed. In the shakedown problem, the solution u to the elasticity equation (23) must exist and be in $H^1(\Omega)$. Since the loading, a traction g located on the boundary Γ_N, is taken in $L^2\left(\partial\Omega, \mathbb{R}^2\right)$, one can conclude that the domain's boundary $\partial\Omega$ is required to be Lipschitz (from the regularity of elliptic equations results [32]). Lemma 4.1 outlines the admissible perturbations within $\Theta_{ad} = W^{1,\infty}\left(\mathbb{R}^2, \mathbb{R}^2\right)$:

Lemma 4.1. *Let Ω_0 be a Lipschitz bounded open set and $\theta \in W^{1,\infty}\left(\mathbb{R}^2, \mathbb{R}^2\right)$. Then, if $\|\theta\|_{W^{1,\infty}} \leq 1$, $I_2 + \theta$ is a diffeomorphism, $(I_2 + \theta)(\Omega_0)$ is a bounded open set with a Lipschitz boundary and $(I_2 + \theta)(\partial\Omega_0) = \partial\left((I_2 + \theta)(\Omega_0)\right)$.*

Note that Lemma 4.1 also requires a condition on the norm of the perturbation, θ. This restriction is not considered in the admissible perturbation domain. Indeed, in this work, the numerical algorithm is based on a gradient descent and thus, on small variations. In this way, a perturbation θ, chosen to be a descent direction, is multiplied by a step ζ to ensure small variations and thus also bound the perturbation. A definition of shape differentiability can now be stated in two dimensions [6, 43, 66].

Definition 4.1. *A functional $J : \Omega \to \mathbb{R}$ is said to be shape differentiable at Ω_0 if the application $\theta \to J\left((I_2 + \theta)(\Omega_0)\right)$ is Fréchet-differentiable at 0 in the Banach space $W^{1,\infty}\left(\mathbb{R}^2, \mathbb{R}^2\right)$, i.e.*

$$\begin{gathered} J\left((I_d + \theta)(\Omega_0)\right) = J(\Omega_0) + DJ(\Omega_0)(\theta) + o(\theta) \quad \textit{with} \\ \lim_{\theta \to 0} \frac{|o(\theta)|}{\|\theta\|} = 0, \end{gathered} \tag{27}$$

where $DJ(\Omega_0)$ is a continuous linear form on $W^{1,\infty}\left(\mathbb{R}^2, \mathbb{R}^2\right)$.

Below, the shape derivatives of two general functions, defined by the integral respectively on the domain Ω and on the domain boundary $\partial\Omega$, are given.

Proposition 4.1. *Let Ω_0 be a smooth bounded open set of $\mathbb{R}^2$. If $f \in W^{1,1}(\mathbb{R}^2)$ and $J : \mathscr{U}_\Omega \to \mathbb{R}$ is defined by:*

$$J(\Omega) = \int_\Omega f(x)dx,$$

then J is differentiable at Ω_0 and, $\forall \theta \in \Theta_{ad}$,

$$DJ(\Omega)(\theta) = \int_{\partial\Omega} f(s)\theta(s) \cdot n(s)ds. \tag{28}$$

Proposition 4.2. *Let Ω_0 be a smooth bounded open set of $\mathbb{R}^2$. If $g \in W^{2,1}(\mathbb{R}^2)$ and $J : \mathscr{U}_\Omega \to \mathbb{R}$ is defined by:*

$$J(\Omega) = \int_{\partial\Omega} g(s)ds,$$

then J is differentiable at Ω_0 and, $\forall \theta \in \Theta_{ad}$,

$$DJ(\Omega)(\theta) = \int_{\partial\Omega} \left(\frac{\partial f}{\partial n} + \kappa f\right) ds, \tag{29}$$

where $\kappa = div(n)$ is the curvature of Ω. This result holds true if $\partial\Omega$ is replaced by Γ, a smooth open subset of $\partial\Omega$ and assumes that $g = 0$ on the surface boundary $\partial\Gamma$.

The proof of these theorems is given in [69, 66, 3]. A last result, stemming from Hadamard's structure theorem and stated by Simon [69], gives that, if two perturbations $\theta_1, \theta_2 \in \Theta_{ad}$ with enough regularity have the same normal trace on the boundary $\partial\Omega$, then, the shape derivatives of a function applied to these perturbations will be the same:

Proposition 4.3. *Let $J \in \mathscr{C}^k(D,\mathbb{R})$, with $k \geq 1$ and $\Omega_0 \subset D$ such that J is differentiable at Ω_0. Set θ_1, $\theta_2 \in W^{k,\infty}\left(\mathbb{R}^2,\mathbb{R}^2\right)$. If Ω_0 is an open bounded set, with $\partial\Omega_0 \in \mathscr{C}^1$, and if:*

$$\begin{cases} \theta_1 - \theta_2 \in \mathscr{C}^k\left(\mathbb{R}^2,\mathbb{R}^2\right), \\ \theta_1 \cdot n = \theta_2 \cdot n \, on \, \partial\Omega_0, \end{cases} \tag{30}$$

then,

$$DJ(\Omega_0)(\theta_1) = DJ(\Omega_0)(\theta_2). \tag{31}$$

A consequence of this theorem is that the derivative of a function applied to a perturbation θ only depends on the normal trace $\theta \cdot n$ at the boundary $\partial\Omega$ and, under some regularity assumption on J, there exists $\mathscr{V} \in L^1(\partial\Omega)$ [33] such that:

$$\forall \theta \in \Theta_{ad}, \quad DJ(\Omega)(\theta) = \int_{\partial\Omega} \mathscr{V}\theta \cdot n ds. \tag{32}$$

To run a descent gradient algorithm, this derivative must be translated into a gradient $\nabla J(\Omega)$. Since the normal component only impacts the shape's variations, we consider $J'(\Gamma) = \nabla J(\Gamma) \cdot n$ and we then would have:

$$J(\Omega(\theta)) = J(\Omega) + \nabla J(\Omega) \cdot \theta + o(\theta) = J(\Omega) + J'(\Omega)\theta \cdot n + o(\theta). \tag{33}$$

It would then be sufficient to choose $\partial\theta = -J'(\Omega) \cdot n$ to make the objective function decrease. From the shape derivative's structure (see eq. (32)), a first choice would be:

$$J'(\Omega) = \begin{cases} \mathscr{V}n & \text{on} \, \partial\Omega \\ 0 & \text{elsewhere,} \end{cases} \tag{34}$$

corresponding to a L^2-scalar product ($W^{1,\infty}(D) \subset L^2(D)$).

As a result, based on eq. (27), the objective function would decrease. However, $\mathscr{V}$ (and thus θ) could lack smoothness. Indeed, in our problem, the only guarantee we have about the solution to eq. (23), is that $u \in H^1(\Omega)$. Due to the possible presence of the gradient of u in the shape derivative, $\mathscr{V} \in L^2(\Omega)$ may no longer be regular enough and θ may be out of the admissible set $W^{1,\infty}$. To address this problem, one should choose the scalar product related to $H^k(D)$, fixing k such that $H^k(D) \subset W^{1,\infty}(D)$. From the Sobolev embedding theorem [32], this requires that, with d the space dimension (2 in this case):

$$k > \frac{d}{2} = 1, \tag{35}$$

and one should choose $k \geq 2$. Considering $k = 2$, we would take $\theta = -J'(\Omega)n$, with $J'(\Omega) \in H^2(D)$ the solution of:

$$\forall W \in H^2(D), \int_D \nabla(\nabla J'(\Omega)) : \nabla(\nabla W) + \nabla Q \cdot \nabla W + J'(\Omega) W dx \tag{36}$$

$$= \int_{\partial\Omega} \mathscr{V} W ds. \tag{37}$$

Solving this equation guarantees the correct regularity for θ. However, the computational cost would also increase drastically. To balance these issues, an alternative intermediate scalar product could be employed [5, 36, 21]. We use here one of the most common, the H^1- scalar product, and $\theta = -J'(\Omega)n$ such that $J'(\Omega)$ is the solution of:

$$\forall W \in H^1(D), \quad \int_D \alpha^2 \nabla J'(\Omega) \cdot \nabla W + J'(\Omega) W dx = \int_{\partial\Omega} \mathscr{V} W ds. \tag{38}$$

Note that the coefficient α is proportional to the characteristic meshsize, Δx [5]. We finally get the following relation between the derivative $DJ(\Omega)$ and the scalar $J'(\Omega)$, the projection of the gradient on the normal to the shape:

$$\forall W \in H^1(\Omega), \qquad DJ(\Omega)(W) = \int_D \alpha^2 \nabla J'(\Omega) \cdot \nabla W + J'(\Omega) W dx = \int_{\partial\Omega} \mathscr{V} W ds, \tag{39}$$

with the final descent direction chosen to be $\theta = -J'(\Omega)n$.

4.2 Level Set Method

Based on the shape differentiation theory outlined above (Section 4.1), different methods to modify the boundaries have been developed, such as homogenization [2, 10] and level-set methods [5]. The latter is selected here. Introduced by Sethian and Osher [71], it has since been widely applied and further developed for shape optimization problems. Let a shape Ω be in $\mathscr{U}_\Omega$. A level set function ψ is then defined such that:

$$\begin{cases} \psi(x) < 0 & \text{if } x \in \Omega \\ \psi(x) = 0 & \text{if } x \in \partial\Omega \cap D \\ \psi(x) > 0 & \text{otherwise} \end{cases} \tag{40}$$

The normal n to the shape Ω is given by $\frac{\nabla\psi}{|\nabla\psi|}$, whereas the curvature κ equals $\operatorname{div}\left(\frac{\nabla\psi}{|\nabla\psi|}\right)$. During iterations, the shape Ω is updated. Recall however that, in this work, only the normal trace of the perturbation matters and an advection velocity v, applied in the normal direction n, is defined such that $v = \theta \cdot n$. Assuming that the shape is evolving in time $t \in \mathbb{R}^+$, the level-set function satisfies, $\forall x(t) \in \partial\Omega(t)$,

$$\psi(t, x(t)) = 0. \tag{41}$$

Differentiating eq. (41) with respect to time and together with the relation between the normal n and the level-set function, one gets the following Hamilton-Jacobi equation that governs the shape evolution:

$$\partial_t \psi + vn|\nabla\psi| = 0. \tag{42}$$

A consequence of applying a Hamilton-Jacobi equation is that the level-set function may become too flat or too steep during iteration. To avoid this problem, after each iteration, the function is regularized by solving the following equation:

$$\begin{cases} \partial_t \psi + \operatorname{sign}(\psi_0)\,(|\nabla\psi| - 1) = 0 & \text{in } D \times \mathbb{R}^+ \\ \psi(t = 0, x) = \psi_0(x) & \text{in } D \end{cases} \tag{43}$$

where ψ_0 is the result of the advection iteration and the solution ψ corresponds to the result of the complete iteration. The optimization algorithms have been implemented in FreeFem^{++}, a numerical computation software [41]. The resolution of the advection equation is based on [20, 46] where the "distance" function of FreeFem^{++} has been used for the redistancing operation.

5 Numerical results

To highlight the features of shape optimization under a shakedown constraint, a comparison of results for a select number of test-case problems is presented. In Section 5.1, two different optimization problems are investigated as base-line test-cases. The first one consists in minimizing the mass and compliance without any constraint on stress or shakedown, assuming a perfectly elastic material. This problem is referred to as the "Elastic Problem". The second one differs only by removing the perfect elasticity assumption and adding the constraint that the solid must not go beyond first-yield. Since a von Mises formulation is used to define the elastic limit (for an elastic-perfectly plastic material), this problem is referred to as "von Mises Problem". In both test-cases, the residual (ρ) plays no role in the objective function and does not impact the results. It is thus not considered and the only optimization variable is the shape (Ω). In contrast, in Section 5.2, the residual stress is the only optimization variable. The shape Ω being fixed, the objective is to optimize the residual stress to reduce the effective stress ($\rho + Ae(u)$) as much as possible and return the effective stress state as close as possible to the elasticity domain. This is done using a projected gradient algorithm on the stress variable ($\tilde{\rho}$, which becomes the residual stress after the projection on the residual stress space). This problem is referred to as "Stress-only Problem". Finally, Section 5.3 considers the optimization of both variables (shape and residual stress variables) to minimize the mass and compliance under shakedown constraints. This last test-case is referred to as "Shakedown Problem".

5.1 Shape optimization of the "Elastic Problem" and the "von Mises Problem"

5.1.1 Problem Statement

We consider the residual stress fixed to 0 ($\tilde{\rho} = 0$ and $\eta = 0$). Thus, the constraint C_0 is deactivated because it is fixed to $C_0 = 0$. The new problem (44) thus amounts to optimizing the shape Ω to minimize the objective function J while satisfying the constraint $C_M = 0$. This corresponds to the "von Mises Problem".

$$\begin{aligned}
&\min_{\Omega} J_{\Omega}(\Omega) = \int_{\Omega} dx + l_C \int_{\Omega} Ae(u) : e(u) dx, \\
&\left[\text{s.t.(Von Mises Problem)} \quad C_M(\Omega) = C_M(\Omega, \tilde{\rho} = 0) = \int_{\Omega} \Phi_p \left(\frac{\sigma_{VM}(Ae(u))}{\sigma_Y^2} \right) dx = 0. \right]
\end{aligned} \tag{44}$$

with $u \in H^1(\Omega)$ solution of (23). Note that removing the constraint C_M leads to the "Elastic Problem". As a result, in the following, not considering the constraint $C_M = 0$ amounts to solving the "Elastic Problem" whereas taking it into account leads to the "von Mises Problem".

To deal with the constraints, an effective unconstrained problem is given [70]:

$$\min_{\Omega} \mathscr{J}_{\Omega}(\Omega) = \int_{\Omega} dx + l_C \int_{\Omega} Ae(u) : e(u) dx + \lambda_{lag} C + \frac{\mu_{lag}}{2} C^2. \tag{45}$$

The Lagrange multiplier λ_{lag} is updated at each iteration such that:

$$\lambda_{lag}^{k+1} = \lambda_{lag}^{k} + C^k \mu_{lag}. \tag{46}$$

Note that choosing $\lambda_{lag} = 0$ and $\mu_{lag} = 0$ leads to, $\forall k \in \mathbb{N}$, $\lambda_{lag}^{k+1} = 0$ and thus, the constraint $C_M = 0$ is not taken into account. This case corresponds to the "Elastic Problem". Any other choice leads to the "von Mises Problem".

Remark 5.1. *The augmented Lagrangian method is one approach to deal with the constraints, in which their satisfaction is ensured at convergence only. This final convergence may not be reached in a finite (reasonable) number of iterations. In the numerical results, the algorithm has been stopped after a finite number of iterations and the constraints' final values are thus not exactly zero but reach an accepted tolerance.*

5.1.2 Differentiation

Proposition 5.1. *The above optimization problem (eq. 45) has the following shape derivative:*

$$\begin{aligned}
D_{\Omega} \mathscr{J}_{\Omega}(\Omega)(\theta) = \int_{\Gamma} \Bigg[& 1 + l_C Ae(u) : e(u) \\
& + (\lambda_{lag} + \mu_{lag} C) \Phi_p \left(\frac{\sigma_{VM}(Ae(u))}{\sigma_Y^2} \right) + Ae(u) : e(p) \Bigg] \theta \cdot n ds.
\end{aligned} \tag{47}$$

where $p = p_1 + p_2$ with $p_1 = -2 l_C u$, and $p_2 \in H^1(\Omega)$ is the solution of:

$$\begin{cases}
-\text{div}(Ae(p_2)) = \frac{\lambda_{lag} + \mu_{lag} C}{\sigma_Y^2} \text{div} \left(\Phi_p' \left(\frac{\sigma_{VM}(Ae(u))}{\sigma_Y^2} \right) A \sigma_{VM}'(Ae(u)) \right) & \text{in} \, \Omega \\
Ae(p_2) \cdot n = - \frac{(\lambda_{lag} + \mu_{lag} C)}{\sigma_Y^2} \Phi_p' \left(\frac{\sigma_{VM}(Ae(u))}{\sigma_Y^2} \right) A \sigma_{VM}'(Ae(u)) \cdot n & \text{on} \, \Gamma \cup \Gamma_N \\
p_2 = 0 & \text{on} \, \Gamma_D.
\end{cases} \tag{48}$$

Proof. From Cea's method [22], we introduce a Lagrangian function:

$$\mathscr{L}_{\Omega}(\Omega, u, p) = \mathscr{J}_{\Omega}(\Omega) + \int_{\Omega} Ae(u) : e(p) dx - \int_{\Gamma_N} g p ds. \tag{49}$$

Differentiating with respect to the variable u gives, $\forall \varphi \in H_D^1(\Omega)$:

$$\begin{aligned}
\partial_u \mathscr{L}(\Omega, u, p)(\varphi) = & 2 l_C \int_{\Omega} Ae(u) : e(\varphi) dx \\
& + \frac{\lambda_{lag} + \mu_{lag} C}{\sigma_Y^2} \int_{\Omega} \Phi_p' \left(\frac{\sigma_{VM}(Ae(u))}{\sigma_Y^2} \right) \sigma_{VM}'(Ae(u)) : Ae(\varphi) dx \\
& + \int_{\Omega} Ae(p) : e(\varphi) dx.
\end{aligned} \tag{50}$$

Setting this derivative to 0 gives the adjoint problem. If u is the solution of eq. (23), then $\forall p$,

$$\mathscr{L}_{\Omega}(\Omega, u, p) = \mathscr{J}_{\Omega}(\Omega). \tag{51}$$

As a result the derivative to the objective function $\mathscr{J}_\Omega$ corresponds to the derivative of the Lagrangian function $\mathscr{L}_\Omega$:

$$\begin{aligned} \frac{d\mathscr{J}_\Omega}{d\Omega}(\Omega)(\theta) &= \frac{d\mathscr{L}_\Omega}{d\Omega}\big(\Omega,u,p\big)(\theta) \\ &= \partial_\Omega \mathscr{L}_\Omega\left(\Omega,u,p\right)(\theta) + < \partial_u \mathscr{L}_\Omega\left(\Omega,u,p\right), \partial_\Omega u(\theta) > . \end{aligned} \tag{52}$$

From its definition, the adjoint function p chosen will cancel $\partial_u \mathscr{L}_\Omega\left(\Omega,u,p\right)$, which simplifies the problem and thus:

$$D_\Omega \mathscr{J}_\Omega\left(\Omega\right)(\theta) = \partial_\Omega \mathscr{L}\left(\Omega,u,p\right)(\theta). \tag{53}$$

The derivative with respect to the shape follows from the application of Proposition 4.1. □ □

5.1.3 Algorithm

The shape is represented by a level set and the normal advection velocity, v_Ω corresponds to the solution of the regularization problem, eq. (38), where the shape derivative is given by eq. (47). To make sure that the velocity v_Ω (or equivalently the perturbation θ) is small enough, it is modulated by a step that is updated at each iteration. Algorithm 1 summarizes the process. Recall that to consider the "Elastic Problem", the multiplier λ_{lag} and the penalization μ_{lag} are set to 0 and remain unchanged throughout the optimization process, whereas in the "von Mises Problem" optimization, λ_{lag} and μ_{lag} are not equal to 0 and the multiplier λ_{lag} is updated after each iteration following eq.46. Note that the tolerance tol is updated with respect to the iterations and will be determined for each numerical application (see section 5). The initial step ζ_Ω^0 is set to 5.

Initialize the shape Ω;
Compute the elastic stress, the volume, the compliance, the constraint C_M and thus the objective function $\mathscr{J}_\Omega$;
Compute the next advection velocity v_Ω (shape derivative $D_\Omega \mathscr{J}_\Omega(\Omega)$ and regularization);
for *each iteration* **do**
    Shape variation (level set advection and redistancing): $\Omega^{n+1} = \Omega^n + \zeta_\Omega^n v_\Omega^n n^n$;
    Compute the elastic stress, volume, compliance, constraint C and objective function;
    if *improvement:* $\mathscr{J}_\Omega^{n+1} \leq \mathscr{J}_\Omega^n * tol^n$ **then**
        Iteration accepted;
        Update the variable Ω;
        Update the Lagrange multiplier λ_{lag};
        Compute the effective objective function;
        Compute the next advection velocity v_Ω (shape derivative $D_\Omega \mathscr{J}_\Omega(\Omega)$ and regularization);
        Update the step: $\zeta_\Omega^{n+1} = \max(1.2\zeta_\Omega^n, \zeta_\Omega^0)$
    end
    else
        Iteration rejected;
        Update of step: $\zeta_\Omega^{n+1} = 0.6\zeta_\Omega^n$
    end
end

Algorithm 1: Algorithm to optimize the shape in the "Elastic Problem" and the "von Mises Problem"

5.2 Optimization of the residual stress (with a fixed shape): "Stress-only Problem"

The optimization with respect to this second variable, the residual stress, is the novelty in elastoplastic stress-based topology optimization that is introduced by incorporating shakedown theorems. Indeed, not only the shape can be modified but also a residual stress in order to satisfy a von Mises yield criterion. In this test-case, the shape is now fixed and the objective is to optimize the residual stress to minimize the Von Mises functions $\sigma_{VM}(\rho)$ and $\sigma_{VM}(\rho + Ae(u))$. In this optimization problem, the mass minimization is not the objective function any longer, the objective is now a weighted sum of what were previously the problem constraints: C_0 and C_M (see Eq. 54). The minimum of this new objective function may not always be equal to 0. When the objective function reaches zero, this would mean that the current structure under consideration allows for the existence of a residual stress satisfying Melan's theorem and thus that the structure would shakedown. However, the shape chosen may not shakedown (i.e. satisfy Melan's theorem), thus preventing a null convergence value of the objective function.

5.2.1 Problem Statement

For this "Stress-Only" test-case, the new optimization problem is the following:

$$\min_{\tilde{\rho}\in\mathscr{U}_{\tilde{\rho}}} J_\rho(\tilde{\rho}) = l_0 C_0(\tilde{\rho}) + l_M C_M(\tilde{\rho}), \tag{54}$$

where

$$C_0(\tilde{\rho}) = \int_\Omega \Phi_p\left(\frac{\sigma_{VM}(\tilde{\rho}-e(\eta))}{\sigma_Y^2}\right)dx, \quad C_M(\tilde{\rho}) = \int_\Omega \Phi_p\left(\frac{\sigma_{VM}(\tilde{\rho}-e(\eta)+Ae(u))}{\sigma_Y^2}\right)dx \tag{55}$$

with $u \in H^1(\Omega)$ the solution of eq. (23) and $\eta \in H^1(\Omega)$ the solution of eq. (24). The coefficients l_0 and l_M are kept constant during the optimization process.

5.2.2 Differentiation

Proposition 5.2. *Differentiating the optimization problem given by eq.* (55) *results in,* $\forall\sigma \in \mathscr{U}_{\tilde{\rho}}$*:*

$$\begin{aligned} D_{\tilde{\rho}}J_\rho(\tilde{\rho})(\sigma) = \int_\Omega \Bigg[& \tfrac{l_0}{\sigma_Y^2}\Phi_p'\left(\tfrac{\sigma_{VM}(\tilde{\rho}-e(\eta))}{\sigma_Y^2}\right)\sigma_{VM}'(\tilde{\rho}-e(\eta)) + \\ & \tfrac{l_M}{\sigma_Y^2}\Phi_p'\left(\tfrac{\sigma_{VM}(\tilde{\rho}-e(\eta)+Ae(u))}{\sigma_Y^2}\right)\sigma_{VM}'(\tilde{\rho}-e(\eta)+Ae(u)) \\ & +e(q)\Bigg] : \sigma ds. \end{aligned} \tag{56}$$

with $q \in H^1(\Omega)$ *the solution of:*

$$\begin{cases} div(e(q)) = & -\frac{l_0}{\sigma_Y^2} div\left(\Phi_p'\left(\frac{\sigma_{VM}(\tilde{\rho}-e(\eta))}{\sigma_Y^2}\right)\sigma_{VM}'(\tilde{\rho}-e(\eta))\right) \\ & -\frac{l_M}{\sigma_Y^2} div\left(\Phi_p'\left(\frac{\sigma_{VM}(\tilde{\rho}-e(\eta)+Ae(u))}{\sigma_Y^2}\right)\sigma_{VM}'(\tilde{\rho}-e(\eta)+Ae(u))\right) & in\,\Omega \\ e(q)\cdot n = & -\frac{l_0}{\sigma_Y^2}\Phi_p'\left(\frac{\sigma_{VM}(\tilde{\rho}-e(\eta))}{\sigma_Y^2}\right)\sigma_{VM}'(\tilde{\rho}-e(\eta))\cdot n \\ & -\frac{l_M}{\sigma_Y^2}\Phi_p'\left(\frac{\sigma_{VM}(\tilde{\rho}-e(\eta)+Ae(u))}{\sigma_Y^2}\right)\sigma_{VM}'(\tilde{\rho}-e(\eta)+Ae(u))\cdot n & on\,\Gamma\cup\Gamma_N \\ q = 0 & & on\,\Gamma_D \end{cases} \tag{57}$$

Proof. The Lagrangian of the problem is, $\forall\tilde{\rho} \in \mathscr{U}_{\tilde{\rho}}$, $\forall\eta,q,u,p \in H_D^1(\Omega)$,

$$\begin{aligned} \mathscr{L}_\rho(\tilde{\rho},\eta,q,u,p) = l_0C_0 + l_MC_M - \int_\Omega e(\eta):e(q) - \tilde{\rho}:e(q)dx \\ + \int_\Omega Ae(u):e(p)dx - \int_{\Gamma_N} gpds. \end{aligned} \tag{58}$$

Differentiating with respect to η and setting this derivative to 0 gives the adjoint equation related to q. As in the case for Section5.1, we notice that, if η is the solution of eq. (24), then $\forall q \in H^1(\Omega)$,

$$\mathscr{L}_\rho(\tilde{\rho},\eta,q) = J_\rho(\tilde{\rho}). \tag{59}$$

This gives that, $\forall\sigma \in \mathscr{U}_{\tilde{\rho}}$:

$$\frac{d\mathscr{L}_\rho}{d\tilde{\rho}}(\tilde{\rho},\eta,q)(\sigma) = \partial_\Omega\mathscr{L}_\rho(\tilde{\rho},\eta,q)(\sigma) + <\partial_\eta\mathscr{L}_\rho(\tilde{\rho},\eta,q),\partial_{\tilde{\rho}}\eta(\sigma)>. \tag{60}$$

From its definition, the adjoint function q chosen will cancel $\partial_\eta\mathscr{L}_\rho(\tilde{\rho},\eta,q)$, simplifying the problem:

$$D_{\tilde{\rho}}J_\rho(\tilde{\rho})(\sigma) = \partial_{\tilde{\rho}}\mathscr{L}_\rho(\tilde{\rho},\eta,q)(\sigma). \tag{61}$$

□ □

5.2.3 Algorithm

The optimization variable is in this case a stress and a descent direction must be found in the stress domain $\mathscr{U}_{\tilde{\rho}}$. Still considering the scalar product given by eq. (15), one could take, $\forall \tilde{\rho}, \sigma \in \mathscr{U}_{\tilde{\rho}}$,

$$D_{\tilde{\rho}} J_\rho(\tilde{\rho})(\sigma) = \int_\Omega J'_\rho(\tilde{\rho}) : \sigma dx = \int_D J'_\rho(\tilde{\rho}) : \sigma dx. \tag{62}$$

Then, a descent direction, v_ρ, in this case could be:

$$\begin{array}{rl} v_\rho = -J'_\rho(\tilde{\rho}) = & -\frac{l_0}{\sigma_Y^2}\Phi'_p\left(\frac{\sigma_{VM}(\tilde{\rho}-e(\eta))}{\sigma_Y^2}\right)\sigma'_{VM}(\tilde{\rho}-e(\eta)) \\ & -\frac{l_M}{\sigma_Y^2}\Phi'_p\left(\frac{\sigma_{VM}(\tilde{\rho}-e(\eta)+Ae(u))}{\sigma_Y^2}\right)\sigma'_{VM}(\tilde{\rho}-e(\eta)+Ae(u)) \\ & -e(q). \end{array} \tag{63}$$

By definition of the operator $e(.)$ (see eq. (2)), $v_\rho \in \mathscr{U}_{\tilde{\rho}}$ is the space of stresses defined on Ω. Algorithm 2 summarizes the optimization process for this test-case. Note that in this test-case, the tolerance is fixed to 1 and the step ζ_ρ^0 is initialized to 1.

```
Compute the elastic stress related to the fixed shape Ω;
Initialize ρ̃;
Project ρ̃ in the space of self-equilibrated stresses (compute η);
Compute C_0, C_M and the objective function J_ρ;
Compute the descent direction in the space U_ρ̃;
for each iteration do
    Stress variation: ρ̃^{n+1} = ρ̃^n + ζ_ρ^n v_ρ^n;
    Project ρ̃ in the space of self-equilibrated stresses (compute η);
    Compute C_0, C_M and the objective function J_ρ;
    if improvement: J_ρ^{n+1} ≤ J_ρ^n then
        Iteration accepted;
        Update the variable ρ̃, the displacement η and the functions C_0, C_M and Jrho;
        Compute the descent direction in the space U_ρ̃;
        Update the step: ζ_ρ^{n+1} = 1.3 ζ_ρ^n
    end
    else
        Iteration rejected;
        Update the step: ζ_ρ^{n+1} = 0.4 ζ_ρ^n
    end
end
```

Algorithm 2: Algorithm to optimize the residual stress only; the shape remains fixed: "Stress-Only" Problem.

5.3 Optimization of both the shape and the residual stress under shakedown constraint: "Shakedown Problem"

The objective is now to optimize both the shape and the residual stress. The approach taken consists in optimizing each of them in an alternating fashion to yield the best combination. The scheme for alternating the variable optimizations chosen here is: doing 1 iteration for the shape, followed by 50 iterations for the stress. Thus, for each intermediary shape, the residual stress obtained is quite close to the optimal one. The step for the shape, ζ_{sh} is initialized to 5. The step related to the stress ζ_ρ is initialized to 1 each time the stress optimization is performed.

5.3.1 Iteration related to the shape

With $\tilde{\rho}$ being fixed, the problem is the following:

$$\begin{array}{rl} \min_\Omega J_{sh}(\Omega,\tilde{\rho}) = & \int_\Omega dx + l_C \int_\Omega Ae(u) : e(u) dx \\ & +\lambda_{lag,0} C_0(\Omega,\tilde{\rho}) + \frac{\mu_{lag,0}}{2} C_0(\Omega,\tilde{\rho})^2 \\ & +\lambda_{lag,M} C_M(\Omega,\tilde{\rho}) + \frac{\mu_{lag,M}}{2} C_M(\Omega,\tilde{\rho})^2. \end{array} \tag{64}$$

with C_0 and C_M defined by eq. (21), and $u, \eta \in H_D^1(\Omega)$ the solutions of eq. (23) and eq. (24), respectively. The coefficient $\lambda_{lag,0}$ and $\lambda_{lag,M}$ are updated at each iteration: $\lambda_{lag,0}^{k+1} = \lambda_{lag,0}^k + C_0^k \mu_{lag,0}$ and $\lambda_{lag,M}^{k+1} = \lambda_{lag,M}^k + C_M^k \mu_{lag,M}$.

Proposition 5.3. *The differentiation of the optimization problem, eq.* (64)*, gives:*

$$D_\Omega J_{sh}(\Omega,\tilde{\rho})(\theta) = \int_\Gamma \Big[\quad 1 + l_C Ae(u) : e(u) + Ae(u) : e(p) - e(v) : e(Q) + \tilde{\rho} : e(Q) \\ + (\lambda_{lag,0} + \mu_{lag,0} C_0)\, \Phi_p \left(\tfrac{\sigma_{VM}(\tilde{\rho} - e(\eta))}{\sigma_Y^2} \right) \\ + (\lambda_{lag,M} + \mu_{lag,M} C_M)\, \Phi_p \left(\tfrac{\sigma_{VM}(\tilde{\rho} - e(\eta) + Ae(u))}{\sigma_Y^2} \right) \Big] \theta \cdot n \, ds. \tag{65}$$

with $p = p_1 + p_2$ *and* $p_1 = -2 l_C u$ *and* $p_2 \in H^1(\Omega)$ *being the solution of:*

$$\begin{cases} -div(Ae(p_2)) = div\left[\dfrac{(\lambda_{lag,M} + \mu_{lag,M} C_M)}{\sigma_Y^2} \Phi_p' \left(\dfrac{\sigma_{VM}(\tilde{\rho} - e(\eta) + Ae(u))}{\sigma_Y^2} \right) A \sigma_{VM}'(\tilde{\rho} - e(\eta) + Ae(u)) \right] & in \quad \Omega \\ Ae(p_2) \cdot n = - \dfrac{(\lambda_{lag,M} + \mu_{lag,M} C_M)}{\sigma_Y^2} \Phi_p' \left(\dfrac{\sigma_{VM}(\tilde{\rho} - e(\eta) + Ae(u))}{\sigma_Y^2} \right) A \sigma_{VM}'(\tilde{\rho} - e(\eta) + Ae(u)) \cdot n & on \quad \Gamma \cup \Gamma_N \\ p_2 = 0 \quad on \quad \Gamma_D. \end{cases} \tag{66}$$

and $Q \in H^1(\Omega)$ *the solution of:*

$$\begin{cases} -div(e(Q)) = div\left[\dfrac{(\lambda_{lag,0} + \mu_{lag,0} C_0)}{\sigma_Y^2} \Phi_p' \left(\dfrac{\sigma_{VM}(\tilde{\rho} - e(v))}{\sigma_Y^2} \right) \sigma_{VM}'(\tilde{\rho} - e(v)) \right] & in\ \Omega \\ \quad + div\left[\dfrac{(\lambda_{lag,M} + \mu_{lag,M} C_M)}{\sigma_Y^2} \Phi_p' \left(\dfrac{\sigma_{VM}(\tilde{\rho} - e(v) + Ae(u))}{\sigma_Y^2} \right) \sigma_{VM}'(\tilde{\rho} - e(v) + Ae(u)) \right] & \\ e(Q) \cdot n = - \dfrac{(\lambda_{lag,0} + \mu_{lag,0} C_0)}{\sigma_Y^2} \Phi_p' \left(\dfrac{\sigma_{VM}(\tilde{\rho} - e(v))}{\sigma_Y^2} \right) \sigma_{VM}'(\tilde{\rho} - e(v)) \cdot n & on\ \Gamma \cup \Gamma_N \\ \quad - \dfrac{(\lambda_{lag,M} + \mu_{lag,M} C_M)}{\sigma_Y^2} \Phi_p' \left(\dfrac{\sigma_{VM}(\tilde{\rho} - e(v) + Ae(u))}{\sigma_Y^2} \right) \sigma_{VM}'(\tilde{\rho} - e(v) + Ae(u)) \cdot n & \\ Q = 0 & on \Gamma_D. \end{cases} \tag{67}$$

5.3.2 Iteration related to the residual stress

For each iteration, once the shape update has been done, the residual stress is optimized. Fifty iterations of a gradient algorithm are performed, corresponding to the optimization problem presented in Section 5.2.

5.3.3 Algorithm

These strategies are summarized by Figure 5. The expected results are the following. First, the relatively unconstrained "Elastic Problem" should result in a smaller volume (mass) than in the "von Mises" constrained case. Indeed, the mass of in the "Elastic Problem" should be the smallest amongst all test-cases considered. As for the "Shakedown Problem" result, it should result in an intermediate volume (mass): larger than the relatively unconstrained elastic test-case and smaller than the traditional von Mises constrained case. Indeed, if properly constrained, the introduction of the stress as an optimization variable gives more freedom to the system.

Second, as the von Mises constraints are being dealt with using an Augmented Lagrangian Method, they should decrease to 0 during the optimization process. It is expected that, at convergence, these constraints are satisfied both in the "von Mises" and in the "Shakedown" problems. In contrast, in the "Elastic Problem", von Mises constraints are not considered in the optimization. Finally, in the case of the "Stress-only Problem", they should decrease during the optimization problem but their minimum could be different from 0. Indeed, as already explained, the shape is fixed in this optimization problem, and may not admit a shakedown solution. If the minimum of the constraints were 0, this would amount to the existence of a residual stress satisfying the assumptions of Melan's theorem, meaning that the structure would shakedown.

Lastly, recall that each result presented below is a local minimum that depends on the optimization process; since these problems are not convex, the unicity of an optimum is not guaranteed. As stated in the introduction, the objective of this work is not to find the best optimization parameters nor to identify the most accurate techniques to deal with elasto-plasticity. Our goal is to reveal, using simple test-cases and established optimization processes, the main differences introduced by employing shakedown theorems and to motivate their further investigation in structural topology optimization. The comparison of the different test-case problems and results is detailed below.

Initialize the shape Ω;
Compute the elastic stress, the volume and the compliance;
Initialize the residual stress $\tilde{\rho}$ at 0 and compute η;
Optimize the objective function $J_\rho = l_0 C_0 + l_M C_M$ by varying the residual stress, while the shape remains fixed;
Using the optimized residual stress $\tilde{\rho}$, compute C_0, C_M, and J_{sh}, the objective function corresponding to eq. (64);
Compute the shape derivative $D_\Omega J_{sh}(\Omega)$ and, after regularization, of the advection velocity v_{sh};
for *each iteration* **do**
    Perform shape variation (level set advection and redistancing): $\Omega^{n+1} = \Omega^n + \zeta_{sh}^n v_{sh}^n n^n$;
    Compute the elastic stress, the volume and the compliance;
    Starting from $\tilde{\rho}^n$, optimize the objective function $J_\rho = l_0 C_0 + l_M C_M$, while the shape remains fixed;
    Using the optimized residual stress $\tilde{\rho}$, compute C_0, C_M, and J_{sh}, the objective function corresponding to eq. (64);
    if *improvement:* $J_{sh}^{n+1} \leq J_{sh}^n * tol^n$ **then**
        Iteration accepted;
        Update the variables Ω and $\tilde{\rho}$;
        Update the Lagrange multipliers $\lambda_{lag,0}$ and $\lambda_{lag,M}$;
        Compute the effective objective function;
        Compute the next advection velocity v_{sh} (shape derivative $D_\Omega \mathscr{J}_\Omega(\Omega)$ and regularization);
        Update the step: $\zeta_{sh}^{n+1} = \max(1.2\zeta_{sh}^n, \zeta_{sh}^0)$
    end
    else
        Iteration rejected;
        Update the step: $\zeta_{sh}^{n+1} = 0.6\zeta_{sh}^n$
    end
end

Algorithm 3: Iterative algorithm to optimize the "Shakedown Problem".

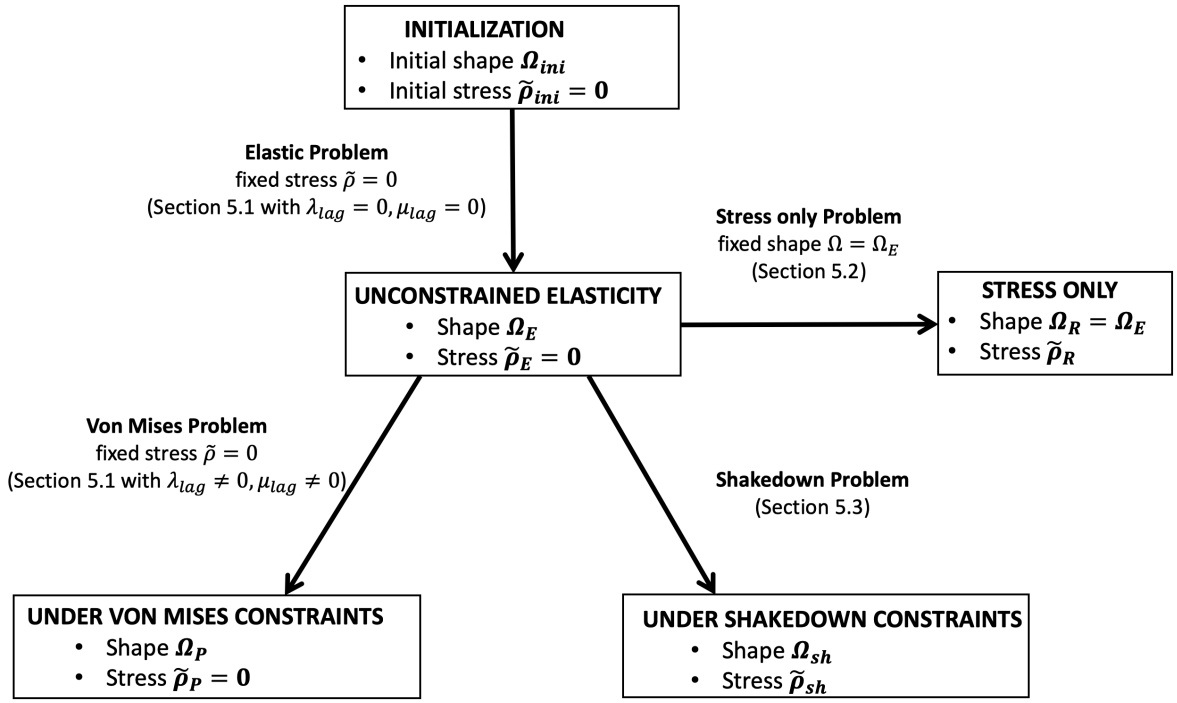

Figure 5: Resolution strategy for test-cases explored.

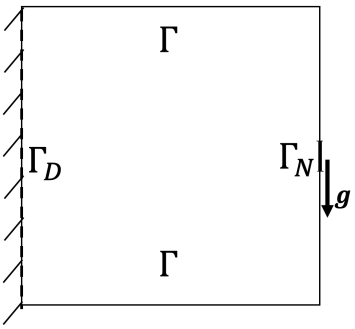

(a) Cantilever test-case

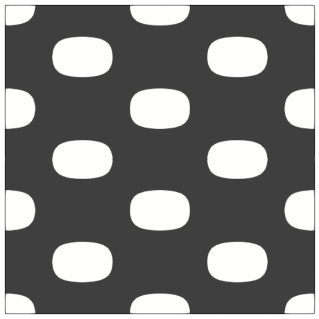

(b) Initial shape (Case I_C)

Figure 6: Cantilever test-case

5.4 Results

5.4.1 Cantilever

We consider the classic cantilever problem. The working domain is a square with a characteristic length of size 2, discretized into 25.600 triangular elements (see Figure 6). The loading is applied on the middle of the right side (centered about a segment of size 0.2). The left side constitutes the Dirichlet boundary, Γ_D. The relevant material properties and design parameters (non-dimensional) are the following: Young's modulus $E = 1960$, Poisson's ratio $\nu = 0.30$, yield stress $\sigma_Y = 0.95$, and loading $g = (0, -1.1)$. Due to symmetry, the computations are done on only one-half of the working domain. The coefficient chosen for the norm is $p = 8$ (see eq. (13)) and the regularization coefficient $\alpha = \Delta x$ (see eq. (38)).
In each of the following cases, the compliance multiplier l_C is arbitrarily fixed to 2000. For the "Elastic Problem", the optimization process is initialized as shown in Figure 6 (black is solid and white is void). Then, the optimization is run with a tolerance initialized to 2 and multiplied by 0.9 every 100 iterations. The test-case is stopped after 300 iterations (chosen with respect to the evolution of the objective function, see Figure 7). In the following, the result of the "Elastic Problem" is referred to as "E_C".

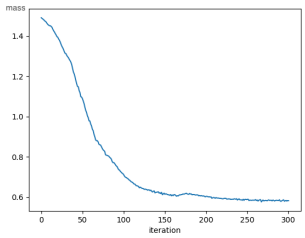

(a) Mass evolution

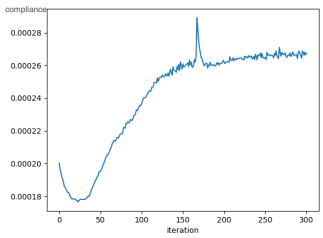

(b) Compliance evolution

Figure 7: Evolution of the mass and compliance with respect to iterations for the "Elastic Problem" in the cantilever application.

Each of the other test-cases is initialized by the result of the "Elastic Problem" (with a regularization first applied, eq.43). In the "von Mises Problem", the Augmented Lagrangian coefficients are initialized to $\lambda_{lag} = 0$ and $\mu_{lag} = 100$. The tolerance is in this case also initialized to 2 and multiplied by 0.9 every 100 iterations. The test is stopped after 300 iterations (see Figure 8 for the convergence). In the following figures, the result of the "von Mises Problem" is referred to as "P_C".

The "Stress-only Problem" is initialized by the result of the "Elastic Problem" and the stress field $\rho = 0$. The coefficients l_0 and l_M are both set to 1. The tolerance is set to 1 (descent only is accepted) and the test is stopped after 300 iterations (see Figure 9 for the convergence). In the following, the result of the "Stress-only Problem" is referred to as "R_C".

Finally, the "Shakedown Problem" is also initialized by the result of the "Elastic Problem" and the stress field $\rho = 0$. The coefficients l_0 and l_M are both set to 1 and the tolerance of the inner loop, focusing on the stress optimization, is set to 1 and stopped after 50 iterations. The Augmented Lagrangian multipliers are initialized to $\lambda_{lag,0} = \lambda_{lag,M} = 10000$ and $\mu_{lag,0} = \mu_{lag,M} = 0$. The optimization is stopped after 99 iterations and the results are referred to as "SH_C". Convergence is not reached at this iteration but the final volume and the constraints C_M are smaller than in the "von Mises Problem". The constraint C_0 remains very small, thus

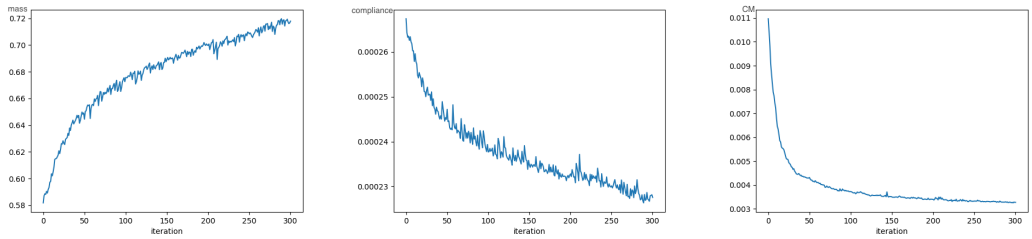

(a) Mass evolution (b) Compliance evolution (c) Constraint C_M evolution

Figure 8: Evolution of the mass, compliance and constraint C_M with respect to iterations for the "von Mises Problem" in the cantilever application.

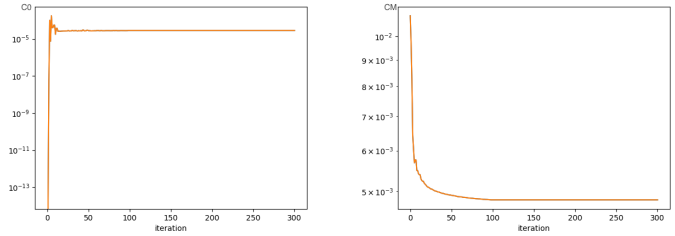

(a) Function C_0 evolution (vertical log scale) (b) Function C_M evolution (vertical log scale)

Figure 9: Evolution of the functions C_0 and C_M with respect to iterations for the "Stress-only Problem" in the cantilever application.

motivating the use of shakedown constraints that allow for a mass reduction from the "von Mises Problem" result while avoiding low-cycle fatigue and other related behaviors (alternating plasticity, ratchetting, collapse). The evolution of the mass, compliance, C_0 and C_M with respect to the optimization is shown in Figure 10.

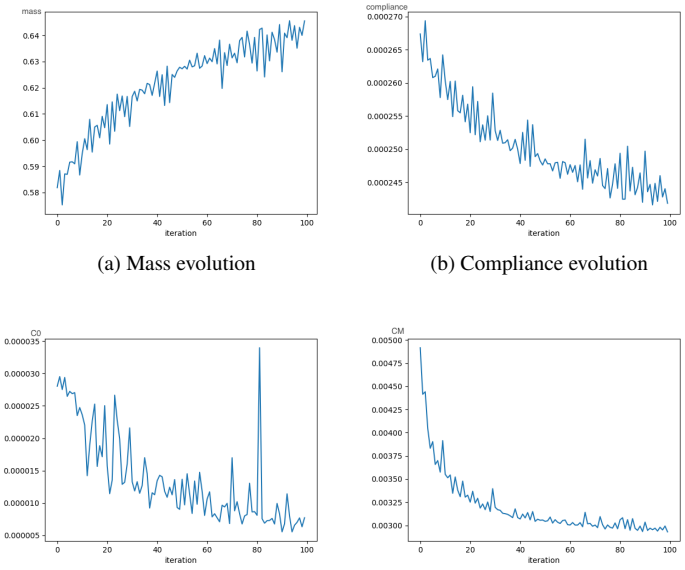

(a) Mass evolution (b) Compliance evolution

(c) Function C_0 evolution (d) Function C_M evolution

Figure 10: Evolution of the functions mass, compliance, C_0 and C_M with respect to iterations for the "Shakedown Problem" in the cantilever application.

The results are summarized in Figure 11 and Table 1. All results are given for the upper half of the cantilever. In Figure 11, each row represents one optimization case (Elastic Problem E_C, Von Mises Problem

P_C, Stress-only Problem R_C or Shakedown Problem SH_C). In the first column, the shape Ω resulting from each optimization is displayed (note that the shape is the same for E_C and R_C since the optimization of the stress only was performed and the R_C problem was initialized by the result of the Elastic Problem and did not involve any changes to the shape). In the second column, the von Mises function for the residual stress ρ is shown (note that since this was not an optimization variable for the Elastic and von Mises Problems, there are no pictures for the first two rows and the residual stress field is kept at 0 during those optimizations). In the third column, the von Mises function for the stress $\rho + Ae(u)$ is displayed (equal to $Ae(u)$ for the first two rows, E_C and P_C). In each of the von Mises figures, the color scale bar below indicates the value of the von Mises function at each point. The color is red if the value is greater than, or equal to, the yield stress σ_Y. Table 1 gives the final values of the volume, the compliance and the constraints C_0 and C_M for each case.

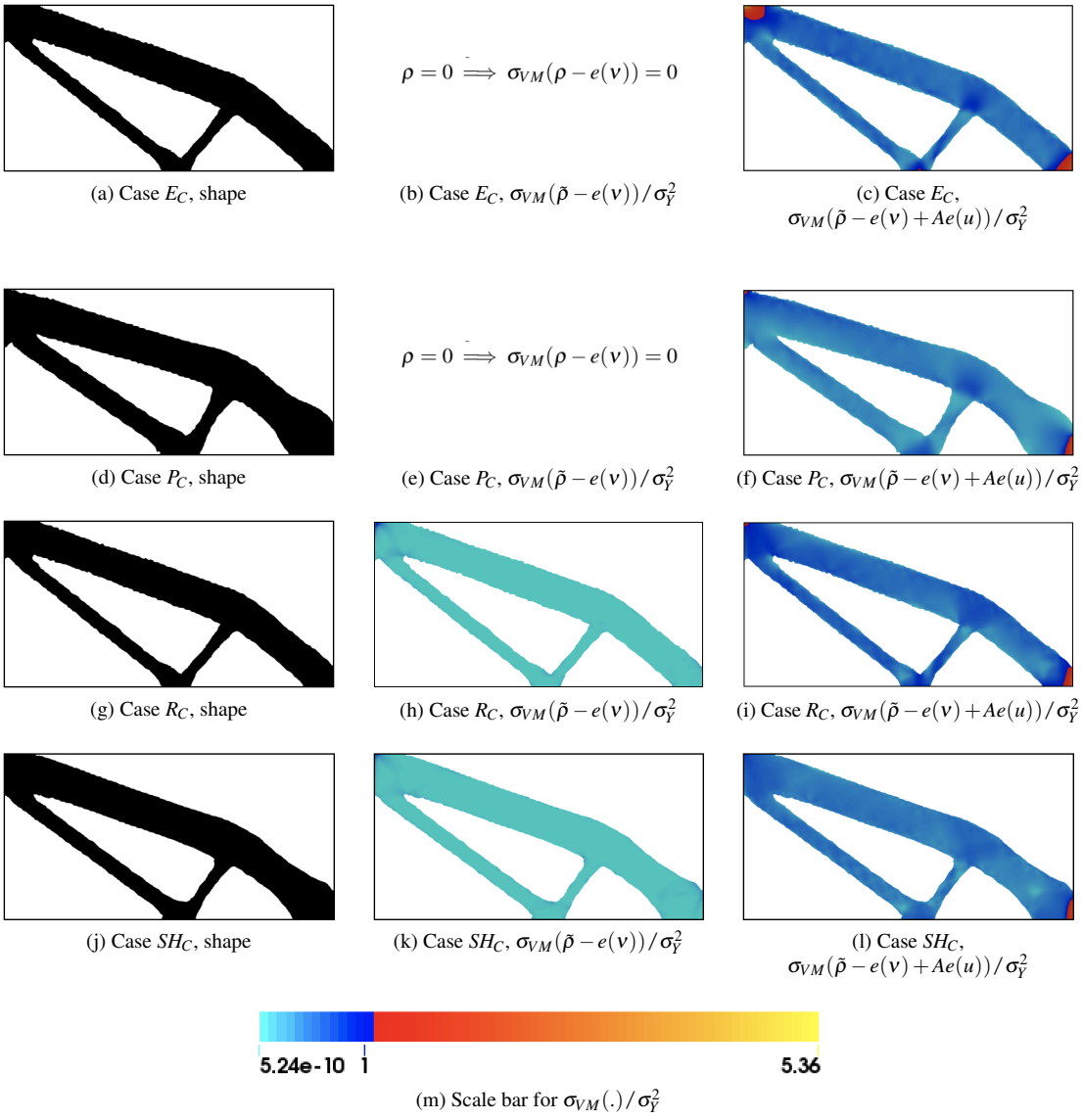

(a) Case E_C, shape

(b) Case E_C, $\sigma_{VM}(\tilde{\rho} - e(v))/\sigma_Y^2$

(c) Case E_C, $\sigma_{VM}(\tilde{\rho} - e(v) + Ae(u))/\sigma_Y^2$

(d) Case P_C, shape

(e) Case P_C, $\sigma_{VM}(\tilde{\rho} - e(v))/\sigma_Y^2$

(f) Case P_C, $\sigma_{VM}(\tilde{\rho} - e(v) + Ae(u))/\sigma_Y^2$

(g) Case R_C, shape

(h) Case R_C, $\sigma_{VM}(\tilde{\rho} - e(v))/\sigma_Y^2$

(i) Case R_C, $\sigma_{VM}(\tilde{\rho} - e(v) + Ae(u))/\sigma_Y^2$

(j) Case SH_C, shape

(k) Case SH_C, $\sigma_{VM}(\tilde{\rho} - e(v))/\sigma_Y^2$

(l) Case SH_C, $\sigma_{VM}(\tilde{\rho} - e(v) + Ae(u))/\sigma_Y^2$

(m) Scale bar for $\sigma_{VM}(.)/\sigma_Y^2$

Figure 11: Summary of the cantilever results.

Case	Description	Volume	Compliance	C_0	C_M
E_C	Elastic Problem	0.582	2.67e-04	0	1.10e-02
R_C	Stress-only Problem	0.582	2.67e-04	2.86e-05	4.82e-03
SH_C	Shakedown Problem	0.646	2.42e-04	7.71e-06	2.93e-03
P_C	von Mises Problem	0.718	2.23e-04	0	3.28e-03

Table 1: Comparison of the final results for all the Cantilever test-case variations.

Based on these results, Table 1 highlights the following:

- The Elastic Problem gives the best result (E_C) with respect to the mass (volume). However, since no constraints were set on the stress, the von Mises function $\sigma_{VM}(Ae(u)$ exceeds the yield stress (with σ_{VM} locally reaching $5.36\sigma_Y^2$, see Figure 11) and the function C_M is far above 0. This corresponds with the expectations since the optimization algorithm did not consider any constraint on the effective von Mises stresses.

- The von Mises Problem (P_C) results in a higher mass than in the Elastic Problem (+23.4%). Actually, this mass is the highest of all of the results. However, the von Mises function remains mostly under the yield stress (red part in the von Mises graphs in Figure 11) and the function C_M is very close to 0. Note that this value is not exactly 0. Indeed, the constraints are dealt with using an Augmented Lagrangian Method which has the particularity that the constraints will only be satisfied at convergence. However, the code has to be stopped after a finite number of iterations which explains the non zero values. Changing the mode of constraints integration is a topic for future work (see Section 7).

- Without any shape modification, the Stress-only optimization (R_C) has the same final mass (volume) as in the Elastic Problem (E_C). However, the introduction of the stress variable allows for a decrease of the von Mises function and the red area in Figure 11k is smaller. Note that the residual stress is different from zero on the top left and the bottom right corners, where the von Mises function in Figure11(i) slightly exceeded the yield stress.

- The Shakedown Problem (SH_C) results in a mass greater than the Elastic Problem (+11.0%) but smaller than in the von Mises Problem (-10%). Indeed, the introduction of the stress variable allowed for more freedom to make the von Mises function remain below the yield stress. Note that in this case again, the final residual stress is different from zero in the top left and bottom right corners (Figure 11l).

5.4.2 L-Bracket

We also consider the L-Bracket problem that is often used as a test-case in stress-based topology optimization. The working domain is a L-shape defined by a square domain of size 2.5 from which a square of size 1.5 has been removed from the top right upper corner. It is meshed with $28,800$ triangular elements (see Figure 12). The upper side constitutes the Dirichlet boundary Γ_D. The loading is applied on the middle of the right side (centered about a segment of size 0.1). The relevant material properties and design parameters (non-dimensional) are the following: Young's modulus $E = 1$, Poisson's ratio $\nu = 0.30$, yield stress $\sigma_Y = 20$, and loading $g = (0, -10)$. The coefficient chosen for the norm is $p = 16$ (see eq. (9)) and the regularization coefficient is $\alpha = 5\Delta x$ (see eq. (38)).

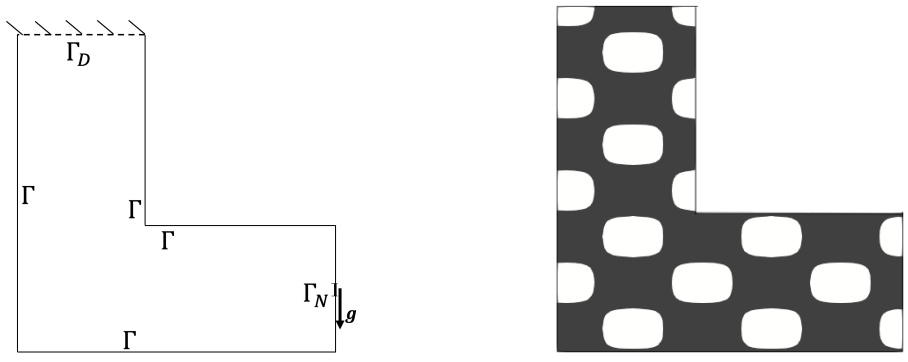

(a) L-Bracket test-case

(b) Initial shape (Case I_{LB})

Figure 12

In each of the following cases, the compliance multiplier l_C is arbitrarily fixed to 0.01. For the Elastic problem, the optimization process is initialized as shown in Figure 12 (black is solid and white is void). Then, the optimization is run with a tolerance initialized to 2 and multiplied by 0.9 every 100 iterations. The test-case is stopped after 499 iterations (chosen with respect to the evolution of the objective function, see Figure 13). In the following, the result of the "Elastic Problem" for the L-Bracket is referred to as "E_{LB}".

Each of the remaining cases is initialized by the result of the Elastic Problem (after a regularization has been applied, eq.43). In the von Mises optimization, the Augmented Lagrangian coefficients are initialized to $\lambda_{lag} = 10000$ and $\mu_{lag} = 0$. The tolerance is in this case also initialized to 1.2 and multiplied by 0.9 every 100 iterations. The test-case is stopped after 300 iterations (see Figure 14 for the convergence) and the results are referred to as "P_{LB}".

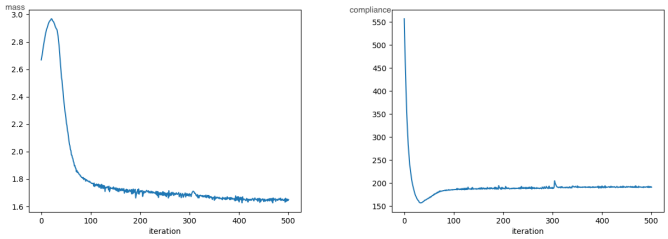

(a) Mass evolution (b) Compliance evolution

Figure 13: Evolution of the mass and compliance with respect to iterations for the Elastic Problem in the L-Bracket case

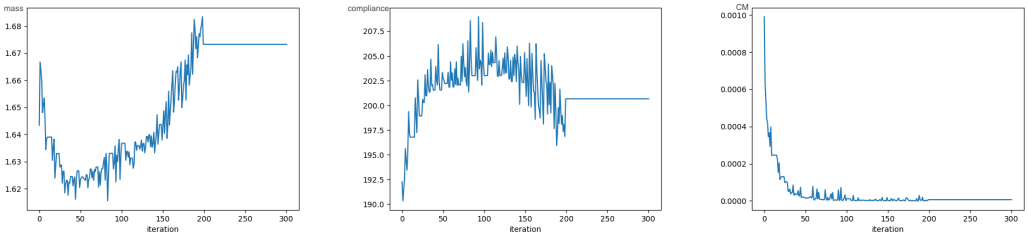

(a) Mass evolution (b) Compliance evolution (c) Constraint C_M evolution

Figure 14: Evolution of the mass, compliance and constraint C_M with respect to iterations for the Von Mises Problem in the L-Bracket case.

The "Stress-only Problem" is initialized by the result of the Elastic Problem and the stress field $\rho = 0$. The coefficients l_0 and l_M are both set to 1. The tolerance is set to 1 (descent only is accepted) and the test-case is stopped after 300 iterations (see Figure 15 for the convergence). In the following, the result of the "Stress-only Problem" for the L-Bracket is referred to as "R_{LB}".

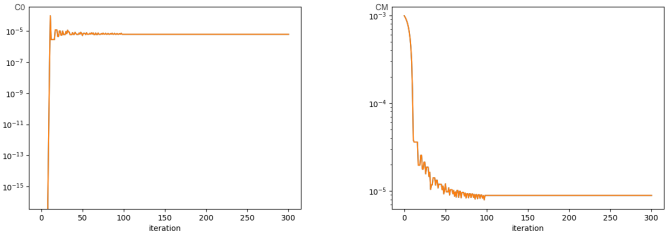

(a) Function C_0 evolution (vertical log scale) (b) Function C_M evolution (vertical log scale)

Figure 15: Evolution of the functions C_0 and C_M with respect to iterations for the Stress-Only Problem in the L-Bracket case

Finally, the Shakedown Problem is initialized by the result of the Elastic Problem and the stress field $\rho = 0$. The coefficients l_0 and l_M are both set to 1 and the tolerance of the inner loop, focusing on the stress optimization, is set to 1 and stopped after 50 iterations. The Augmented Lagrangian multipliers are initialized to $\lambda_{lag,0} = \lambda_{lag,M} = 10000$ and $\mu_{lag,0} = \mu_{lag,M} = 0$. The optimization is stopped after 88 iterations and the results are referred to as "SH_{LB}". In this case again, the convergence is not reached at this iteration (88) but the final volume and the constraints C_M are smaller than in the von Mises Problem and the constraint C_0 remains very small. The evolution of the mass, compliance, C_0 and C_M with respect to the optimization is shown in Figure 16.

The results are summarized in Figure 17 and Table 2. In Figure 17, each row represents one optimization case (E_{LB}, P_{LB}, R_{LB} and SH_{LB}). On the first column, the shape Ω resulting of each optimization is displayed (note that the shape is the same for E_{LB} and R_{LB} since the optimization of the Stress-only Problem was initial-

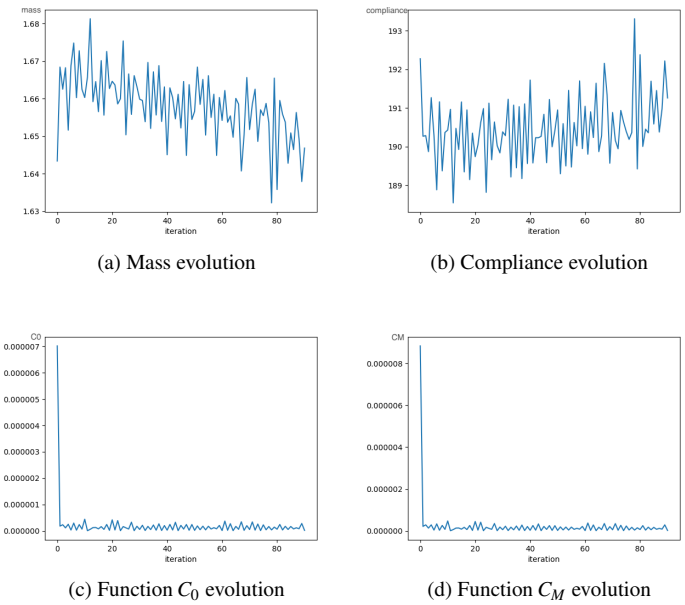

(a) Mass evolution

(b) Compliance evolution

(c) Function C_0 evolution

(d) Function C_M evolution

Figure 16: Evolution of the functions mass, compliance, C_0 and C_M with respect to iterations for the Shakedown Problem in the L-Bracket case

ized by the result of the Elastic Problem and did not involve the shape). On the second column, the von Mises function of the residual stress ρ is shown (note that since this was not an optimization variable for the Elastic and von Mises problems, there are no pictures for the two first rows and the residual stress field is kept at 0 during the optimization). On the third column, the von Mises function of the stress $\rho + Ae(u)$ is displayed (equal to $Ae(u)$ for the two first columns). In each of the von Mises figures, the color scale gives the value of the von Mises function at each point. The color is red if the value is greater than, or equal to, the yield stress σ_Y. Table 2 gives the final values of the volume, the compliance and the constraints C_0 and C_M for each test-case.

Case	Description	Volume	Compliance	C_0	C_M
E_{LB}	Elastic Problem	1.64	192	0	9.91e-04
R_{LB}	Stress only Problem	1.64	192	6.19e-06	8.89e-06
SH_{LB}	Shakedown Problem	1.65	191	8.46e-08	8.56e-08
P_{LB}	von Mises Problem	1.67	201	0	6.41e-06

Table 2: Comparison of the final results for all the L-Bracket test-case variations.

Based on these results, Table 2 highlights the following:

- Here again, the Elastic Problem gives the best result (E_{LB}) with respect to the mass (volume). Note that the von Mises function is extremely high in the internal corner of the L-bracket (with σ_{VM} reaching $2.54\sigma_Y^2$ see Figure 17, which is actually the only point at which the von Mises function is above the yield stress).

- The von Mises Problem (P_{LB}) results in a higher mass (volume) than in the Elastic Problem (+1.8%). In this case again, this mass is the worst. However, the difference is a lot smaller than in the cantilever case which is mainly due to the stress accumulation at the internal corner which complicates the optimization (see [81] for further details). Note that, in order to reduce the stress in this corner, the algorithm has actually removed some material from this corner to smooth the shape.

- In the Stress-only optimization (R_{LB}), the introduction of the stress variable allows for a decrease of the von Mises function and the red area in Figure 17i is smaller. Note that this residual stress is not zero at the internal corner, which is expected.

- The Shakedown Problem (SH_C) results in a mass (volume) greater than the Elastic Problem (+0.61%) but smaller than in the von Mises Problem (-1.20%). The difference is again very small. Note that in this case too, the final residual stress is non-zero in the top left and bottom right corners (Figure 17l) .

6 Discussion

The performance benefits of designing to shakedown have been demonstrated for cases with prescribed loading levels in Section 5 and Figures 11 and 17. The results follow the expectations outlined at the end of Section 5.3.3. Indeed, ordering the various test-cases in terms of largest to smallest volume (mass) as is done in Table 1 and Table 2, one can see that the shakedown result is always between the relatively unconstrained elastic result and the von Mises constrained ones. Note that since no shape modification is allowed in the Stress-Only optimization, it is not relevant to compare its mass. In addition, the constraint on plastic behavior $\left(\sigma_{VM}\left(\frac{\rho+Ae(u)}{\sigma_Y^2}\right)\right)$ for shakedown $(\rho \neq 0)$ are quite similar to those in the von Mises constrained cases $(\rho = 0)$, and lower than for the Elastic Problem and for the Stress-Only Problem. The results presented here are based on a relatively straightforward optimization process and it would be of interest to improve the optimization set-up. Indeed, elasto-plastic shape optimization is still being developed and, using better techniques, it could be possible to get closer to the global minima. This would lead to improved final designs and quantification of the mass reduction provided by the use of shakedown. Moreover, the loading and test cases chosen here are quite academic: this work could be expanded, for example, to identify durability benefits from shakedown for structures subject to uncertain loading levels (within a given envelope). Nevertheless, even with these simple test-cases, it is quite clear that the inclusion of shakedown constraints for lightweighting and durability has further potential to be explored.

Another design consideration that should be taken into account in future work is the allowable levels of deformation. Allowing shakedown of the material better leverages a material's load-bearing reserve, however the limited plastic accumulation experienced may, in some cases, lead to unacceptable permanent structural deformations. As the lower bound shakedown limit theorem applied in this study does not include information about the load-history and path-dependent effects that classical incremental approaches provide, additional constraints on allowable deformations may not be directly applied. Instead future research efforts could exploit several bounding techniques from above for shakedown deformations that have been developed and surveyed [26, 54, 60, 83, 84, 86, 59, 17, 58]. Finally, while the work presented here is subject to the same assumptions made for use of Melan's Lower Bound Theorem (see Section 2.1), it is also of interest to incorporate extensions of Melan's theorem or alternative shakedown analysis techniques in shape and topology optimization frameworks for temperature-dependent properties, hardening, creep, damage, nonlinear geometry effects, and others [78, 76, 24, 13, 1, 54, 102, 101, 80, 103].

7 Conclusions

A new approach for incorporating classic plastic design theorems (Melan's lower bound for shakedown) in modern topology opmitimzation is presented. The approach uses level set based topology optimization to capitolize on the mathematical freedom granted by Melan's theorem, in which only the existence of certain residual stress fields based on elastic solutions are required to guarantee asymptotic elastoplastic behavior (shakedown). Cantilever and L-Bracket test-cases are used to demonstrate the utility of designing to shakedown instead of first-yield (using a traditional von Mises constraint). In both problems under prescribed loading conditions, reductions in weight (volume) are identified (-10% for the Cantilever and -1% for the L-Bracket), motivating the further development of such design frameworks.

8 Acknowledgements

Dr. Vermaak would like to acknowledge that this material is based, in part, upon work supported by the United States Air Force Office of Scientific Research (AFOSR) under award number FA9550-16-1-0438 and the AFOSR Summer Faculty Fellowship Program. M. Boissier would like to thank Grégoire Allaire for his crucial guidance and critiques, as well as Georgios Michailidis, Alex Ferrer and Samuel Amstutz for valuable discussions and suggestions during the pursuit of this work.

9 Replication of results

All algorithmic details are given in the paper. If any further information is required, readers can directly ask the authors.

10 Conflict of interest

The authors declare no conflicts of interest.

11 References

References

[1] HF Abdalla, Maher YA Younan, and MM Megahed. "Shakedown limit load determination for a kinematically hardening 90 ° pipe bend subjected to steady internal pressures and cyclic bending moments". In: *Journal of Pressure Vessel Technology* 133 (2011), pp. 051212–1–10.

[2] G Allaire. *Shape Optimization by the Homogenization Method*. Springer Science & Business Media, 2002.

[3] G Allaire and A Craig. *Numerical analysis and optimization: an introduction to mathematical modelling and numerical simulation*. Oxford University Press, 2007.

[4] G Allaire and F Jouve. "Minimum stress optimal design with the level set method". In: *Engineering Analysis with Boundary Elements* 32 (2008), pp. 909–918.

[5] G Allaire, F Jouve, and AM Toader. "Structural Optimization Using Sensitivity Analysis and a Level-Set Method". In: *Journal of Computational Physics* 194.1 (2004), pp. 363–393.

[6] G Allaire and M Schoenauer. *Conception optimale de structures*. Vol. 58. Springer, 2007.

[7] S Amstutz and AA Novotny. "Topological Optimization of Structures Subject to Von Mises Stress Constraints". In: *Structural and Multidisciplinary Optimization* 41.3 (2010), pp. 407–420.

[8] *ASME Boiler and Pressure Vessel Code*. New York: ASME, 2003.

[9] MR Begley and AG Evans. "Progressive Cracking of a Multilayer System Upon Thermal Cycling". In: *Journal of Applied Mechanics* 68.4 (2001), pp. 513–520.

[10] MP Bendsøe and O Sigmund. *Topology optimization: theory, methods and applications*. Ed. by Springer Verlag. Springer, 2004.

[11] S Benfratello, L Palizzolo, and P Tabbuso. "Optimization of structures with unrestricted dynamic shakedown constraints". In: *Structural and Multidisciplinary Optimization* 52.3 (2015), pp. 431–445.

[12] H Bleich. "Über die Bemessung statisch unbestimmter Stahltragwerke unter Berücksichtigung des elastisch-plastischen Verhaltens des Baustoffes". In: *Bauingenieur* 19.20 (1932), pp. 261–266.

[13] M Boulbibane and ARS Ponter. "A method for the evaluation of design limits for structural materials in a cyclic state of creep". In: *European Journal of Mechanics-A/Solids* 21 (2002), pp. 899–914.

[14] AF Bower. *Applied mechanics of solids*. CRC Press, 2009.

[15] J Bree. "Elastic-plastic behaviour of thin tubes subjected to internal pressure and intermittent high-heat fluxes with application to fast-nuclear-reactor fuel elements". In: *The Journal of Strain Analysis for Engineering Design* 2.3 (1967), pp. 226–238.

[16] J Bree. "Incremental growth due to creep and plastic yielding of thin tubes subjected to internal pressure and cyclic thermal stresses". In: *The Journal of Strain Analysis for Engineering Design* 3.2 (1968), pp. 122–127.

[17] J Bree. "Plastic deformation of a closed tube due to interaction of pressure stresses and cyclic thermal stresses". In: *International Journal of Mechanical Sciences* 31.11-12 (1989), pp. 865–892.

[18] M Bruggi. "On an alternative approach to stress constraints relaxation in topology optimization". In: *Structural and multidisciplinary optimization* 36.2 (2008), pp. 125–141.

[19] *BS 5500: British standard specification for fusion welded pressure vessels*. London: British Standards Institute, 1996.

[20] C Bui, C Dapogny, and P Frey. "An Accurate Anisotropic Adaptation Method for Solving the Level Set Advection Equation". In: *International Journal for Numerical Methods in Fluids* 70.7 (2012), pp. 899–922.

[21] M Burger. "A Framework for the Construction of Level Set Methods for Shape Optimization and Reconstruction". In: *Interfaces and Free Boundaries* 5 (2002), pp. 301–329.

[22] J Céa. "Conception optimale ou identification de formes: calcul rapide de la dérivée directionnelle de la fonction cout". In: *Modélisation mathématique et analyse numérique* 20 (1986), pp. 371–402.

[23] J Chakrabarty. *Theory of plasticity*. Elsevier, 2012.

[24] H Chen. "Lower and upper bound shakedown analysis of structures with temperature-dependent yield stress". In: *Journal of Pressure Vessel Technology* 132.1 (2010), p. 011202.

[25] GD Cheng and X Guo. "ε-relaxed approach in structural topology optimization". In: *Structural Optimization* 13.4 (1997), pp. 258–266.

[26] L Corradi. "Mathematical programming methods for displacement bounds in elasto-plastic dynamics". In: *Nuclear Engineering and Design* 37.1 (1976), pp. 161–177.

[27] JD Deaton and RV Grandhi. "Stress-based design of thermal structures via topology optimization". In: *Structural and Multidisciplinary Optimization* 53.2 (2016), pp. 253–270.

[28] P Duysinx and MP Bendsøe. "Topology optimization of continuum structures with local stress constraints". In: *International journal for numerical methods in engineering* 43.8 (1998), pp. 1453–1478.

[29] P Duysinx and O Sigmund. "New developments in handling stress constraints in optimal material distribution". In: *Proc of the 7th AIAA/USAF/NASAISSMO Symp on Multidisciplinary Analysis and Optimization*. Vol. 1. 1998, pp. 1501–1509.

[30] P Duysinx et al. "Topology and generalized shape optimization: why stress constraints are so important?" In: *International Journal for Simulation and Multidisciplinary Design Optimization* 2.4 (2008), pp. 253–258.

[31] W Egner, Z Kordas, and M Zyczkowski. "Optimal plastic shape design via the boundary perturbation method". In: *Structural optimization* 8.2-3 (1994), pp. 145–155.

[32] LC Evans. *Partial Differential Equations*. Vol. 19. Graduate Studies in Mathematics. American Mathematical Society, Providence, RI, 1998.

[33] Allaire G Feppon F and Dapogny C. "Null space gradient flows for constrained optimization with applications to shape optimization". In: *SIAM Journal on Applied Mathematics* In preparation. (2018).

[34] F Giambanco, L Palizzolo, and L Cirone. "Computational methods for optimal shakedown design of FE structures". In: *Structural optimization* 15.3-4 (1998), pp. 284–295.

[35] F Giambanco, L Palizzolo, and C Polizzotto. "Optimal shakedown design of beam structures". In: *Structural optimization* 8.2-3 (1994), pp. 156–167.

[36] F de Gournay. "Velocity Extension for the Level-Set Method and Multiple Eigenvalues in Shape Optimization". In: *SIAM Journal on Control and Optimization* 45.1 (2006), pp. 343–367.

[37] M Grüning. *Die Tragfähigkeit statisch unbestimmter tragwerke aus stahl bei beliebig häufig wiederholter belastung*. Springer, 1926.

[38] F Gu et al. "Characterization and prediction of permanent deformation properties of unbound granular materials for pavement ME design". In: *Construction and Building Materials* 155 (2017), pp. 584–592.

[39] X Guo et al. "Stress-related topology optimization via level set approach". In: *Computer Methods in Applied Mechanics and Engineering* 200.47 (2011), pp. 3439–3452.

[40] J Haslinger and R Mäkinen. "Shape optimization of elasto-plastic bodies under plane strains: sensitivity analysis and numerical implementation". In: *Structural optimization* 4.3-4 (1992), pp. 133–141.

[41] F Hecht. "New Development in FreeFem++". In: *J. Numer. Math.* 20.3-4 (2012), pp. 251–265.

[42] M Heitzer et al. "Shakedown and ratchetting under tension–torsion loadings: analysis and experiments". In: *Nuclear Engineering and Design* 225.1 (2003), pp. 11–26.

[43] A Henrot and M Pierre. *Shape Variation and Optimization*. Vol. 28. EMS Tracts in Mathematics. European Mathematical Society (EMS), Zürich, 2018.

[44] I Hlaváček. "Shape optimization of elastoplastic bodies obeying Hencky's law". In: *Aplikace matematiky* 31.6 (1986), pp. 486–499.

[45] E Holmberg, B Torstenfelt, and A Klarbring. "Stress constrained topology optimization". In: *Structural and Multidisciplinary Optimization* 48.1 (2013), pp. 33–47.

[46] *ISCDtoolbox/Advection*. ISCD toolbox, 2018. URL: `https://github.com/ISCDtoolbox/Advection` (visited on 10/18/2019).

[47] Z Kammoun and H Smaoui. "A direct approach for continuous topology optimization subject to admissible loading". In: *Comptes Rendus Mécanique* 342.9 (2014), pp. 520–531.

[48] Z Kammoun and H Smaoui. "A direct method formulation for topology plastic design of continua". In: *Direct Methods for Limit and Shakedown Analysis of Structures*. Springer, 2015, pp. 47–63.

[49] J Kato et al. “Analytical sensitivity in topology optimization for elastoplastic composites”. In: *Structural and Multidisciplinary Optimization* 52.3 (2015), pp. 507–526.

[50] WT Koiter. “General theorems for elastic-plastic solids”. In: *Progress in solid mechanics* (1960), pp. 167–221.

[51] JA König. *Shakedown of elastic-plastic structures*. Elsevier, The Netherlands, 1987.

[52] JA König and G Maier. “Shakedown analysis of elastoplastic structures: a review of recent developments”. In: *Nuclear Engineering and design* 66.1 (1981), pp. 81–95.

[53] C Le et al. “Stress-Based Topology Optimization for Continua”. In: *Structural and Multidisciplinary Optimization* 41.4 (2010), pp. 605–620.

[54] FA Leckie. “Review of bounding techniques in shakedown and ratcheting at elevated temperature”. In: *Weld. Res. Counc. Bull.;(United States)* 195 (1974).

[55] E Lee, KA James, and JRRA Martins. “Stress-Constrained Topology Optimization with Design-Dependent Loading”. In: *Structural and Multidisciplinary Optimization* 46.5 (2012), pp. 647–661.

[56] J Lubliner. *Plasticity theory*. Courier Corporation, 2008.

[57] Y Luo and Z Kang. “Topology optimization of continuum structures with Drucker–Prager yield stress constraints”. In: *Computers & Structures* 90 (2012), pp. 65–75.

[58] G Maier and E Vitiello. “Bounds on plastic strains and displacements in dynamic shakedown of work-hardening structures”. In: *Journal of Applied Mechanics* 41.2 (1974), pp. 434–440.

[59] G Maier et al. *Bounds and Estimates on Inelastic Deformations*. Tech. rep. Commission of the European Communities Reports WGCS-AG2, RA1-016-I and RA1-0168-D, 1996.

[60] JB Martin. *Plasticity: fundamentals and general results*. MIT press, 1975.

[61] A Maury, G Allaire, and F Jouve. “Elasto-Plastic Shape Optimization Using the Level Set Method”. In: *SIAM Journal on Control and Optimization* 56.1 (2018), pp. 556–581.

[62] K Maute, S Schwarz, and E Ramm. “Adaptive topology optimization of elastoplastic structures”. In: *Structural and Multidisciplinary Optimization* 15.2 (1998), pp. 81–91.

[63] A Mazzù and G Donzella. “A model for predicting plastic strain and surface cracks at steady-state wear and ratcheting regime”. In: *Wear* 400 (2018), pp. 127–136.

[64] E Melan. “Der Spannungszustand eines Mises-Henckyschen Kontinuums bei veraenderlicker Belastung”. In: *Sitzber. Akad. Wiss.* 147 (1938), pp. 73–78.

[65] E Melan. “Zur Plastizität des räumlicken Kontinuums”. In: *Ing. Arch.* 8 (1938), pp. 116–126.

[66] G Michailidis. “Manufacturing Constraints and Multi-Phase Shape and Topology Optimization via a Level-Set Method”. PhD. Ecole Polytechnique, 2014, pp. 1–277.

[67] P Michaleris, DA Tortorelli, and CA Vidal. “Tangent operators and design sensitivity formulations for transient non-linear coupled problems with applications to elastoplasticity”. In: *International Journal for Numerical Methods in Engineering* 37.14 (1994), pp. 2471–2499.

[68] F Murat and J Simon. “Etude de Problemes d’optimal Design”. In: *Optimization Techniques Modeling and Optimization in the Service of Man Part 2*. Ed. by G Goos et al. Vol. 41. Springer Berlin Heidelberg, 1976, pp. 54–62.

[69] F Murat and J Simon. “Sur le contrôle par un domaine géométrique”. In: *Publication du Laboratoire d’Analyse Numérique de l’Université Paris* 6 (1976), p. 189.

[70] J Nocedal and SJ Wright. *Numerical optimization*. Springer Science+ Business Media, 2006.

[71] S Osher and J Sethian. “Fronts Propagating with Curvature-Dependent Speed: Algorithms Based on Hamilton-Jacobi Formulations”. In: *Journal of Computational Physics* 79.1 (1988), pp. 12–49.

[72] L Palizzolo and P Tabbuso. “Reliability-based design optimization of trusses under dynamic shakedown constraints”. In: *Structural and Multidisciplinary Optimization* 60.3 (2019), pp. 1097–1108.

[73] J Parıés et al. “Block aggregation of stress constraints in topology optimization of structures”. In: *Advances in Engineering Software* 41.3 (2010), pp. 433–441.

[74] J Parıés et al. “Topology Optimization of Continuum Structures with Local and Global Stress Constraints”. In: *Structural and Multidisciplinary Optimization* 39.4 (2009), pp. 419–437.

[75] CBW Pedersen. “Topology optimization of 2D-frame structures with path-dependent response”. In: *International Journal for Numerical Methods in Engineering* 57.10 (2003), pp. 1471–1501.

[76] M Peigney. “On Melan’s theorem in temperature-dependent viscoplasticity”. In: *Models, Simulation, and Experimental Issues in Structural Mechanics*. Springer, 2017, pp. 167–186.

[77] M Peigney. “On shakedown of shape memory alloys structures”. In: *Annals of Solid and Structural Mechanics* 6.1-2 (2014), pp. 17–28.

[78] M Peigney. “Shakedown of elastic-perfectly plastic materials with temperature-dependent elastic moduli”. In: *Journal of the Mechanics and Physics of Solids* 71 (2014), pp. 112–131.

[79] JT Pereira, EA Fancello, and CS Barcellos. “Topology Optimization of Continuum Structures with Material Failure Constraints”. In: *Structural and Multidisciplinary Optimization* 26.1 (2004), pp. 50–66.

[80] DC Pham. “Consistent limited kinematic hardening plasticity theory and path-independent shakedown theorems”. In: *International Journal of Mechanical Sciences* 130 (2017), pp. 11–18.

[81] R Picelli et al. “Stress-Based Shape and Topology Optimization with the Level Set Method”. In: *Computer Methods in Applied Mechanics and Engineering* 329 (2018), pp. 1–23.

[82] Nuclear Electric PLC. *R5 Assessment procedure for the high temperature response of structures*. Nuclear Electric PLC, 1990.

[83] ARS Ponter. “An upper bound on the small displacements of elastic, perfectly plastic structures”. In: *Journal of Applied Mechanics* 39.4 (1972), pp. 959–963.

[84] ARS Ponter. “General bounding theorems for the quasi-static deformation of a body of inelastic material, with applications to metallic creep”. In: *Journal of Applied Mechanics* 41.4 (1974), pp. 947–952.

[85] ARS Ponter, AD Hearle, and KL Johnson. “Application of the kinematical shakedown theorem to rolling and sliding point contacts”. In: *Journal of the Mechanics and Physics of Solids* 33.4 (1985), pp. 339–362.

[86] ARS Ponter, RR Jakeman, and CJ Morrison. “An experimental study of simplified methods for the prediction of the deformation of structures subject to severe cyclic thermal loading”. In: *The Journal of Strain Analysis for Engineering Design* 20.4 (1985), pp. 225–240.

[87] W Prager. “Problem types in the theory of perfectly plastic materials”. In: *Journal of the Aeronautical Sciences* 15.6 (1948), pp. 337–341.

[88] E Rohan and JR Whiteman. “Shape optimization of elasto-plastic structures and continua”. In: *Computer Methods in Applied Mechanics and Engineering* 187.1-2 (2000), pp. 261–288.

[89] S Schwarz, K Maute, and E Ramm. “Topology and shape optimization for elastoplastic structural response”. In: *Computer Methods in Applied Mechanics and Engineering* 190.15 (2001), pp. 2135–2155.

[90] RW Sharp and JR Booker. “Shakedown of pavements under moving surface loads”. In: *Journal of Transportation Engineering* 110.1 (1984), pp. 1–14.

[91] B Simoens et al. “Analysis of the Dynamic Response of a Controlled Detonation Chamber”. In: *Journal of Pressure Vessel Technology* 133.5 (2011), p. 051209.

[92] B Simoens et al. “Experimental demonstration of shakedown in a vessel submitted to impulsive loading”. In: *Journal of Pressure Vessel Technology* 134 (2012), pp. 1–6.

[93] H Sun et al. “Stabilizing shape memory alloy actuator performance through cyclic shakedown: An empirical study”. In: *The 15th International Symposium on: Smart Structures and Materials & Nondestructive Evaluation and Health Monitoring*. International Society for Optics and Photonics. 2008, p. 69300.

[94] PS Symonds. “Shakedown in continuous media”. In: *Journal of Applied Mechanics-Transactions of the ASME* 18.1 (1951), pp. 85–89.

[95] PS Symonds and W Prager. “Elastic-plastic analysis of structures subjected to loads varying arbitrarily between prescribed limits”. In: *Journal of Applied Mechanics-Transactions of the ASME* 17.3 (1950), pp. 315–323.

[96] F Tin-Loi. “Optimum shakedown design under residual displacement constraints”. In: *Structural and Multidisciplinary Optimization* 19.2 (2000), pp. 130–139.

[97] MN Tran and MR Hill. “Shakedown Analysis of Post-Weld Residual Stress in a Pressurizer Surge Nozzle Full-Scale Mockup”. In: *ASME 2016 Pressure Vessels and Piping Conference*. American Society of Mechanical Engineers. 2016, V06BT06A084–V06BT06A084.

[98] N Vermaak et al. “Advances in Direct Methods for Materials and Structures”. In: ed. by Alan R. S. Ponter Alan Cocks Olga Barrera. Springer International Publishing, 2018. Chap. Some Graphical Interpretations of Melan’s Theorem for Shakedown Design, pp. 179–198.

[99] MY Wang and L Li. “Shape equilibrium constraint: a strategy for stress-constrained structural topology optimization”. In: *Structural and Multidisciplinary Optimization* 47.3 (2013), pp. 335–352.

[100] P Wei, MY Wang, and X Xing. “A study on X-FEM in continuum structural optimization using a level set model”. In: *Computer-Aided Design* 42.8 (2010), pp. 708–719.

[101] D Weichert. “Shakedown at finite displacements; a note on Melan’s theorem”. In: *Mechanics Research Communications* 11.2 (1984), pp. 121–127.

[102] D Weichert and A Hachemi. “Influence of geometrical nonlinearities on the shakedown of damaged structures”. In: *International Journal of Plasticity* 14.9 (1998), pp. 891–907. URL: http://www.sciencedirect.com/science/article/pii/S0749641998000357.

[103] D Weichert and A Ponter. “A historical view on shakedown theory”. In: *The History of Theoretical, Material and Computational Mechanics-Mathematics Meets Mechanics and Engineering*. Springer, 2014, pp. 169–193.

[104] K Wiechmann, F-J Barthold, and E Stein. “Shape optimization under shakedown constraints”. In: *Inelastic Analysis of Structures under Variable Loads*. Springer, 2000, pp. 49–68.

[105] K Wiechmann and E Stein. “Shape optimization for elasto-plastic deformation under shakedown conditions”. In: *International Journal of Solids and Structures* 43.22 (2006), pp. 7145–7165.

[106] SK Wong, A Kapoor, and JA Williams. “Shakedown limits on coated and engineered surfaces”. In: *Wear* 203 (1997), pp. 162–170.

[107] HS Yu and J Wang. “Three-dimensional shakedown solutions for cohesive-frictional materials under moving surface loads”. In: *International Journal of Solids and Structures* 49.26 (2012), pp. 3797–3807.

[108] W Zaki et al. “High-cycle fatigue criterion for shape memory alloys based on shakedown theory”. In: *ASME 2016 Conference on Smart Materials, Adaptive Structures and Intelligent Systems*. American Society of Mechanical Engineers. 2016, V002T03A015–V002T03A015.

[109] X Zheng, H Chen, and Z Ma. “Shakedown boundaries of multilayered thermal barrier systems considering interface imperfections”. In: *International Journal of Mechanical Sciences* 144 (2018), pp. 33–40.

[110] Y Zhuang and K Wang. “Shakedown solutions for pavement structures with von Mises criterion subjected to Hertz loads”. In: *Road Materials and Pavement Design* 19.3 (2018), pp. 710–726.

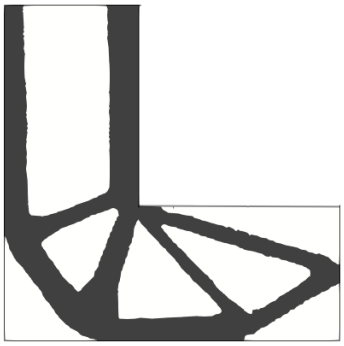

(a) Case E_{LB}, shape

$\rho = 0 \implies \sigma_{VM}(\rho - e(v)) = 0$

(b) Case E_{LB}, $\sigma_{VM}(\tilde{\rho} - e(v))/\sigma_Y^2$

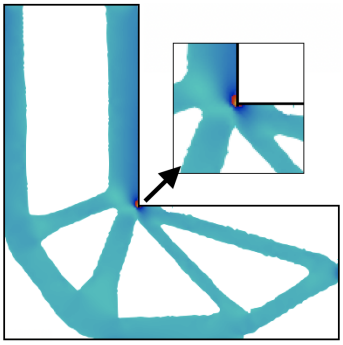

(c) Case E_{LB}, $\sigma_{VM}(\tilde{\rho} - e(v) + Ae(u))/\sigma_Y^2$

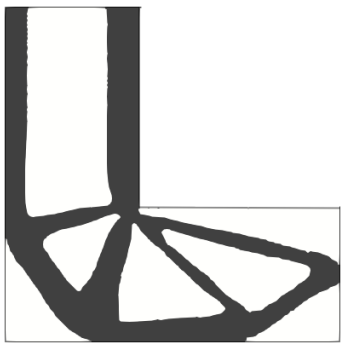

(d) Case P_{LB}, shape

$\rho = 0 \implies \sigma_{VM}(\rho - e(v)) = 0$

(e) Case P_{LB}, $\sigma_{VM}(\tilde{\rho} - e(v))/\sigma_Y^2$

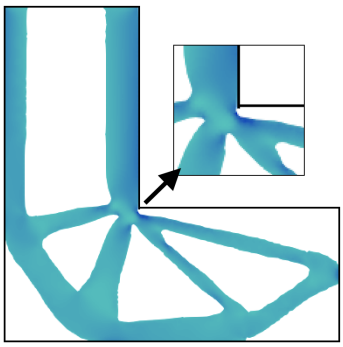

(f) Case P_{LB}, $\sigma_{VM}(\tilde{\rho} - e(v) + Ae(u))/\sigma_Y^2$

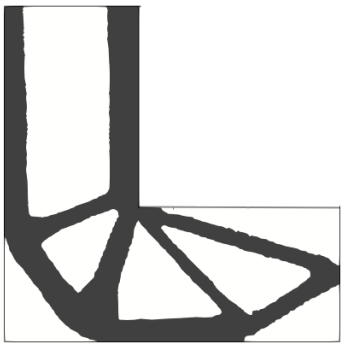

(g) Case R_{LB}, shape

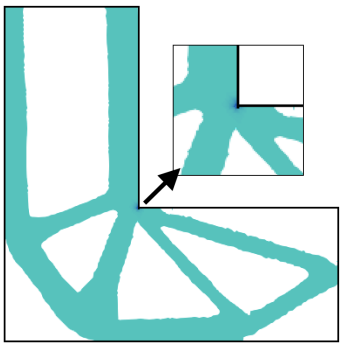

(h) Case R_{LB}, $\sigma_{VM}(\tilde{\rho} - e(v))/\sigma_Y^2$

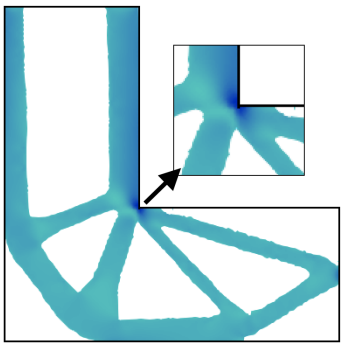

(i) Case R_{LB}, $\sigma_{VM}(\tilde{\rho} - e(v) + Ae(u))/\sigma_Y^2$

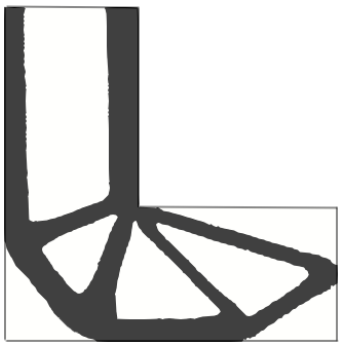

(j) Case SH_{LB}, shape

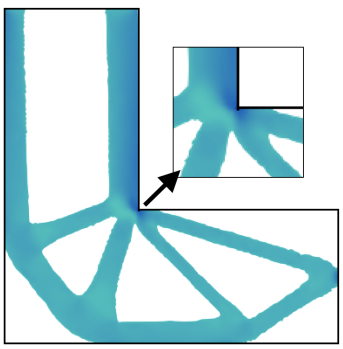

(k) Case SH_{LB}, $\sigma_{VM}(\tilde{\rho} - e(v))/\sigma_Y^2$

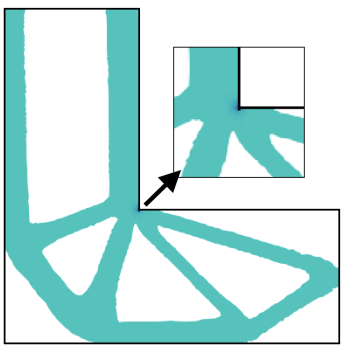

(l) Case SH_{LB}, $\sigma_{VM}(\tilde{\rho} - e(v) + Ae(u))/\sigma_Y^2$

(m) Scale bar for $\sigma_{VM}(.)/\sigma_Y^2$

Figure 17: Summary of the L-Bracket results.